

Chimeric HDAC and the cytoskeleton inhibitor broxbam as a novel therapeutic strategy for liver cancer

SOFIA ISOLDE BÄR¹, ALEXANDRA DITTMER², BIANCA NITZSCHE², GOHAR TER-AVETISYAN³,
MICHAEL FÄHLING³, ADRIAN KLEFENZ⁴, LEONARD KAPS⁴, BERNHARD BIERSACK¹,
RAINER SCHOBERT¹ and MICHAEL HÖPFNER²

¹Organic Chemistry Laboratory, University of Bayreuth, D-95447 Bayreuth;
Institutes of ²Physiology and ³Vegetative Physiology, Charité-Universitätsmedizin Berlin,
Corporate member of Freie Universität Berlin, Humboldt-Universität zu Berlin and Berlin
Institute of Health, D-10117 Berlin; ⁴Institute of Translational Immunology,
University Medical Center of the Johannes Gutenberg University, D-55131 Mainz, Germany

Received September 7, 2021; Accepted February 11, 2022

DOI: 10.3892/ijo.2022.5363

Abstract. Broxbam, also known as *N*-hydroxy-4-{1-methoxy-4-[4'-(3'-bromo-4',5'-dimethoxyphenyl)-oxazol-5'-yl]-2-phenoxy}butanamide, is a novel chimeric inhibitor that contains two distinct pharmacophores in its molecular structure. It has been previously demonstrated to inhibit the activity of histone deacetylases (HDAC) and tubulin polymerisation, two critical components required for cancer growth and survival. In the present study, the potential suitability of broxbam for the treatment of liver cancer was investigated. The effects of broxbam on cell proliferation and apoptosis, in addition to the underlying molecular mechanism of action, were first investigated in primary liver cancer cell lines Huh7, HepG2, TFK1 and EGI1. Real-time proliferation measurements made using the iCEL-Ligence system and viable cell number counting following crystal violet staining revealed that broxbam time- and dose-dependently reduced the proliferation of liver cancer cell lines with IC₅₀ values <1 μM. In addition, a significant inhibition of the growth of hepatoblastoma microtumours on the

chorioallantoic membranes (CAM) of fertilised chicken eggs by broxbam was observed according to results from the CAM assay, suggesting antineoplastic potency *in vivo*. Broxbam also exerted apoptotic effects through p53- and mitochondria-driven caspase-3 activation in Huh7 and HepG2 cells according to data from western blotting (p53 and phosphorylated p53), mitochondrial membrane potential measurements (JC-1 assay) and fluorometric caspase-3 measurements. Notably, no contribution of unspecific cytotoxic effects mediated by broxbam were observed from LDH-release measurements. HDAC1, -2, -4 and -6 expression was measured by western blotting and the HDAC inhibitory potency of broxbam was next evaluated using subtype-specific HDAC enzymatic assays, which revealed a largely pan-HDAC inhibitory activity with the most potent inhibition observed on HDAC6. Silencing HDAC6 expression in Huh7 cells led to a drop in the expression of the proliferation markers Ki-67 and E2F3, suggesting that HDAC6 inhibition by broxbam may serve a predominant role in their antiproliferative effects on liver cancer cells. Immunofluorescence staining of cytoskeletal proteins (α -tubulin & actin) of broxbam-treated HepG2 cells revealed a pronounced inhibition of tubulin polymerisation, which was accompanied by reduced cell migration as determined by wound healing scratch assays. Finally, data from zebrafish angiogenesis assays revealed marked antiangiogenic effects of broxbam *in vivo*, as shown by the suppression of subintestinal vein growth in zebrafish embryos. To conclude, the pleiotropic anticancer activities of this novel chimeric HDAC- and tubulin inhibitor broxbam suggest that this compound is a promising candidate for liver cancer treatment, which warrants further pre-clinical and clinical evaluation.

Correspondence to: Dr Bianca Nitzsche, Institute of Physiology, Charité-Universitätsmedizin Berlin, Corporate member of Freie Universität Berlin, Humboldt-Universität zu Berlin and Berlin Institute of Health, 1 Charitéplatz, D-10117 Berlin, Germany
E-mail: bianca.nitzsche@charite.de

Abbreviations: CA-4, combretastatin A-4; CAM, chorioallantoic membrane; CCC, cholangiocellular carcinoma; GLUT2, glucose transporter 2; HCC, hepatocellular carcinoma; HDAC, histone deacetylase; HDACi, histone deacetylase inhibitor; IC₅₀, mean inhibitory concentration; LDH, lactate dehydrogenase; MMP, mitochondrial membrane potential; SIV, subintestinal veins

Key words: hepatocellular carcinoma, cholangiocellular carcinoma, chimeric histone deacetylase inhibitor, tubulin polymerisation inhibitor

Introduction

The 5-year survival rate of patients with liver cancer (20%) is among the lowest compared with other types of cancer (1). Hepatocellular carcinoma (HCC) and cholangiocellular carcinoma (CCC) are two of the most important types of

primary liver cancers, with HCC being the most common, which accounts for 70-90% of all types of liver cancer (2,3). By contrast, CCC accounts for ~10% of all liver malignancies (2,3). Although CCC is comparatively rare, they are highly aggressive and are typically characterised by poor 5-year survival rates, specifically 5-15% (2,3). The standard systemic therapeutic strategy for HCC is by using the multi-kinase inhibitor sorafenib, which remains unchanged over the last decade (4-7). However, adverse side effects, coupled with the increasing incidence of resistance, are posing significant therapeutic obstacles that needs to be overcome for the effective treatment of HCC (4-7). In addition, currently available treatment options for CCC are even more limited. At early stages surgical tumour resection is a curative option, but only palliative measures are available for advanced and metastatic CCC (8,9). Therefore, treatment possibilities remain limited, which induce severe side effects and only marginally increase the survival time (8,9). There is an urgent demand for novel treatment options for patients with advanced HCC or CCC.

One potential approach of tackling the therapeutic resistance and metabolic evasiveness of cancer cells is the development of 'chimeric inhibitors', which has been garnering interest over recent years (10,11). Using the advent of molecular hybridisation, two distinct drug pharmacophores can be merged into a single molecule, which can simultaneously attack different cellular and molecular targets (10,11). Due to their extensively researched structure-activity relationships, histone deacetylase inhibitors (HDACi) are at the centre of this chimeric drug approach. In recent years, chimeric agents featuring HDACi pharmacophores linked to either protein kinase inhibitors, modulators of the DNA structure or to moieties that can interfere with the cancer cell cytoskeleton, have been developed (11).

HDACs are amidohydrolases that serve a pivotal role in cellular chromatin remodelling (12). They have been previously implicated in the epigenetic regulation of cell metabolism, proliferation and differentiation of various solid cancers, such as urothelial, cervical, myeloma, ovarian and lung cancer, where they have already been tested in early-stage clinical trials (12,13). In several malignancies, including liver cancer, HDACs were found to be overexpressed, where their activity was also correspondingly enhanced (14). In turn, they stifle the expression of tumour suppressor genes, leading to uncontrolled cell division and insensitivity to cell repair mechanisms and suppression of apoptosis (14). Therefore, HDACi are regarded to be promising novel compounds for the therapy of a number of cancers, including liver cancer (14-16). In particular, vorinostat was the first HDACi to be clinically approved for the treatment of T-cell lymphoma (16-18).

Recently, combined treatment with the new HDACi resminostat and the established liver cancer drug sorafenib was reported to effectively counteract HCC growth and progression (19). Similarly, a synergistic inhibitory effect on the proliferation of HT-29 and HCT116 colon cancer cells has been reported for the combination of HDACi and microtubule disrupting agents (MDAs) (20). MDAs trigger the upregulation of p53 and enhance post-translational modifications on p53, such as phosphorylation and acetylation, in non-small lung cancer cells (21). In this regard, potentiation of apoptosis mediated by the combined treatment of the

o-phenylenediamine-based HDACi MS-275 (entinostat) with the MDA taxol combretastatin (CA-4) was previously reported in MCF7 (breast cancer) and HCT (colon cancer) cell lines (22). Treatment with this drug combination led to a pronounced inhibition of tubulin polymerisation to impede neovascularisation and disrupt the tumour vasculature (23). These previous findings aforementioned therefore argue for the acceleration in the development of therapeutic agents that can simultaneously address \geq one target. Drugs that can accomplish this by the means of several covalently-linked pharmacophores are called chimeric drugs (24). Recently, the chimeric inhibitor animacroxam, which induces both HDAC inhibition and cytoskeleton-interfering effects, has been shown to be particularly efficacious against testicular germ cell cancer (15).

Broxbam is a promising chimeric HDACi inhibitor. The pleiotropic effects of broxbam have been previously reported in the 518A2 melanoma cell line, where it was demonstrated to inhibit tubulin polymerisation and HDAC activity, disrupt the cytoskeleton and induce cell cycle arrest (20). Broxbam contains the structural hydroxamate motif of 1st generation HDACi that can also be found on vorinostat in addition to the trimethoxyphenyl motif commonly found on cytostatic MDAs, such as combretastatin A-4 (CA-4) (23,25). In particular, the oxazole bridge of the trimethoxyphenyl motif stabilizes the *cis*-configuration of the alkene (Fig. 1), which is essential for the attachment to the colchicine-binding site of tubulin heterodimers (26). It was recently shown that broxbam can exert antiproliferative effects in melanoma and colorectal cancer cell models (20). However, its potential suitability and efficacy against liver cancer remain poorly understood. Therefore, the present study aims to investigate the effects of broxbam on the physiology of liver cancer cells and the underlying molecular mechanism of action using both *in vivo* and *in vitro* models.

Materials and methods

Compounds. Broxbam was synthesized according to literature (20). In brief, Van Leusen reaction of the 3-bromo-4,5-dimethoxyphenyl toluenesulfonylmethyl isocyanide reagent with ethyl 4-(1-methoxy-4-formyl-2-phenoxy) butyrate led to the ester-functionalised oxazole intermediate, which was reacted with hydroxylamine to form the target compound broxbam. Stock solutions (20 μ M) of broxbam and vorinostat (cat. no. V-8477; LC Laboratories), were prepared in DMSO (Thermo Fisher Scientific, Inc.) stored at -20°C and diluted to the final concentration in fresh media before each experiment. In all experiments, the final DMSO concentration was <0.2%.

Cell culture. HepG2 (hepatoma; DSMZ no. ACC 180), Huh7 (hepatocellular carcinoma; RRID, CVCL_0336), TFK1 [cholangiocellular carcinoma; Deutsche Sammlung von Mikroorganismen und Zellkulturen (DSMZ) no. ACC 344] and EGI1 (cholangiocellular carcinoma; DSMZ no. ACC 385) cells, in addition to the non-transformed hepatocyte cell line non-transformed hepatocyte cell line AML12 (cat. no. CRL-2254) (27) were purchased from ATCC Company and stored for long time in liquid nitrogen in an in-house repository. Only cells in the early passages (<30 passages) were used

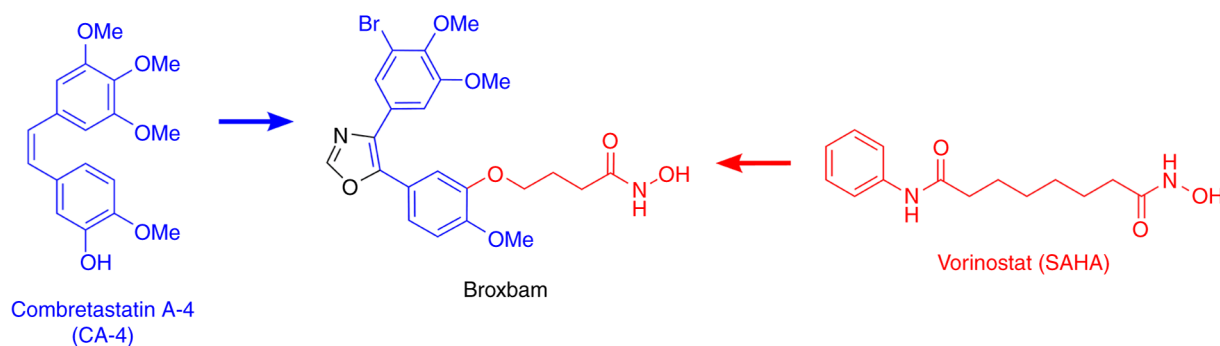


Figure 1. Molecular structures of Broxbam and vorinostat. Structures of the vascular disrupting agents combretastatin A-4 (CA-4), the histone deacetylase-inhibitor vorinostat (red) and the oxazole-bridged hybrid compound broxbam.

for the study. The liver cancer cell lines are representative for the established hepatocellular carcinoma, hepatoblastoma and cholangiocarcinoma cell models for the *in vitro* research of liver cancer (28-32). The murine non-transformed hepatocyte cell line AML-12 (33,34) was used instead of a non-transformed human hepatocyte cell model, which was not available for the present study. However, AML-12 cells represent a widely applied non-transformed hepatocyte cell model (33,34).

The cells were maintained in RPMI 1640 medium containing 10% FBS and 100 U/ml penicillin and streptomycin (all from Gibco, Thermo Fisher Scientific, Inc.) and cultured at 37°C and 5% CO₂ in a humidified atmosphere unless stated otherwise. Cell lines were serially passaged after trypsinisation, using 0.05% trypsin/0.02% EDTA solution (Bio & SELL GmbH). Only mycoplasma-free cultures were used and potential contamination was routinely monitored. Glucose and lactate levels from the cell culture supernatants were measured using a blood gas analyser (ABL800 Flex; Radiometer GmbH).

Small-interfering (si)RNA transfection. For the siRNA-mediated knockdown of HDAC6, Huh7 cells were seeded into six-well plates and cultured until they reached 40-50% confluency. Cells were then transfected with siRNAs (75 nM; ON-TARGET plus SMART pool human HDAC6, cat. no. L-003499-00-0010 or ON-TARGET plus non-targeting control pool, cat. no. D-001810-10-05; PerkinElmer, Inc.; <https://horizondiscovery.com/en/gene-modulation/knockdown/sirna/products/on-target-plus-sirna-reagents?nodeid=entrezgene-10013&catalognumber=L-003499-00-0010>) using the transfection reagent DharmaFECT1 (cat. no. T-2005-01) according to the protocol provided by Dharmacon; PerkinElmer, Inc. In the present study, SMART pool siRNAs targeting human HDAC6 and the non-targeting control containing a mixture of four oligonucleotides were used. The target sequences for human HDAC6 are as follows: Sequence (Seq1, 5'-GGGAGGUUCUUGUGAGAUC-3'; Seq2, 5'-GGAGGUCCUUAUCGUAG A-3'; Seq3, 5'-GCAGUAAAUGAAUCCAU-3' and Seq4, 5'-GUUCACAGCCUAGAAUAUA-3'. Non-targeting control sequences are as follows: Seq1, 5'-UGGUUUACAUGUCGACUAA-3'; Seq2, 5'-UGGUUUACAUGUUGUGUGA-3'; Seq3, 5'-UGGUUUACAUGUUUCUGA-3' and Seq4, 5'-UGGUUUACAUGUUUCCUA-3'. After 48 h of transfection, cells

were harvested and analysed by western blotting and reverse-transcription-quantitative PCR (RT-qPCR).

Crystal violet assay. Changes in cell numbers associated with drug treatment were monitored using crystal violet staining as previously described (35). In total, 1,500-3,000 cells/well were first seeded into 96-well plates and allow to detach for 72 h at 37°C, 5% CO₂ and 95% humidity. The cells were then treated with either broxbam or vorinostat in the following concentrations: 0.1, 0.2, 0.4, 0.8, 1.6, 3.2, 6.4 and 10.0 μM for 24, 48 and 72 h at 37°C, 5% CO₂ and 95% humidity, fixed with 1% glutaraldehyde for 30 min at room temperature and stained with 0.1% crystal violet (Sigma-Aldrich; Merck KGaA) for 30 min at room temperature. Water rinsing was then performed to remove any unbound dye, before 0.2% Triton-X100 was added to solubilise the bound crystal violet and the absorbance at 570 nm was measured using a microplate reader (Dynex Technologies). The light absorbance was assumed in linear proportion to the number of cells.

Real-time inhibition of cell proliferation. The measurement of cell proliferation in real-time was performed as previously described (15). Briefly, HepG2, Huh7 (1.0x10⁴ cells/well), TFK1 (5x10³ cells/well) and EG11 (3x10³ cells/well) cells were seeded into in eight-well E-plates (ACEA Biosciences, Inc.) and maintained under normal cell culture conditions for 24 h. After attachment of the cells, they were treated with concentrations of broxbam (0.1, 0.25, 0.5 and 1.0 μM) for ≤70 h at 37°C, 5% CO₂ and 95% humidity. An impedance-based iCELLigence system (RTCA Software Vs 2.1.0, ACEA Biosciences) was used to monitor the real-time proliferation of viable cells in the eight-well plates at 37°C, 5% CO₂ and 95% humidity, every 15 min for 70 h. Cell proliferation was recorded as a unitless parameter called the 'cell index', which was defined as $(R_{in}-R_{i0})/4.6 \text{ Ohm}$, with R_{in} representing the measured resistance at time point n and R_{i0} representing the background resistance measured at time point T₀.

Lactate dehydrogenase (LDH) cytotoxicity assay. Cells were seeded into 96-well microtiter plates at a density of 8x10³ cells/well and treated with increasing concentrations (0.1, 0.3, 0.6, 1.5, 3.0 and 10.0 μM) of broxbam for 24 h at 37°C, 5% CO₂ and 95% humidity. Cytoplasmic LDH release into the cell culture medium was measured using a colorimetric

assay kit (cat. no. 11644793001; Sigma-Aldrich; Merck KGaA) according to the manufacturers' protocols (36).

Induction of chorioallantoic membrane (CAM) tumours. In total 2×10^6 HepG2 cells were resuspended in $10 \mu\text{l}$ RPMI medium containing 10% FBS and 100 U/ml penicillin and streptomycin (all from Gibco; Thermo Fisher Scientific, Inc.) and $10 \mu\text{l}$ Matrigel (BD Biosciences), before the cell suspension was applied into a silicone ring 5 mm in diameter onto the CAM of fertilised white Leghorn chicken eggs (*Gallus domesticus*) at day 8 of their embryonic development. Fertilized eggs were obtained from Valo Biomedica GmbH (Cuxhaven, Germany) and the embryonic development was induced by incubating the eggs at 37.5°C and 80% humidity as described earlier (37). The tumour-bearing chicken eggs were incubated for 24 h at 37.5°C to stimulate tumour formation, followed by the topical application of $20 \mu\text{l}$ PBS containing three concentrations of broxbam (1.2, 3.0 and $5.0 \mu\text{M}$). After an incubation period of 72 h at 37.5°C and 80% humidity, the tumours were excised and carefully weighed to determine their mass.

Apoptosis detection

Measurement of caspase-3 activity. HepG2 and Huh7 cells were incubated (37°C , 5% CO_2 and 95% humidity) for 48 h in RPMI growth medium (Gibco; Thermo Fisher Scientific, Inc.) containing the respective concentrations of test compounds (0.1, 0.3, 0.6 and $1.2 \mu\text{M}$). The cells were rinsed twice with PBS. All cells were lysed with $500 \mu\text{l}$ lysis buffer (10 mM Tris-HCl, 10 mM $\text{NaH}_2\text{PO}_4/\text{Na}_2\text{HPO}_4$, 130 mM NaCl, 1% Triton X-100 and 10 mM NaPPi, pH 7.5) per 100 cells. Protein concentration was determined using a BCA protein assay kit (Pierce; Thermo Fisher Scientific, Inc.). The activity of caspase-3 was measured using the fluorogenic substrate AC-DEVD-AMC (cat. no. 14987; Cayman Chemical Company). In brief, the cell lysate was adjusted to a protein concentration of 500 mg/ml before $100 \mu\text{l}$ of this cell lysate were mixed with $100 \mu\text{l}$ substrate solution (20 $\mu\text{g}/\text{ml}$ caspase-3 substrate AC-DEVD-AMC, 20 mM HEPES, 10% glycerol and 2 mM DTT, pH 7.5; Sigma-Merck; Merck KGaA). The samples were then incubated for 1 h at 37°C . The fluorescence of the substrate, cleaved by caspase-3, (excitation wavelength=380 nm, emission wavelength=460 nm) was measured using a Varioskan Flash fluorometer (Thermo Fisher Scientific, Inc.).

Detection of changes in the mitochondrial membrane potential (MMP) HepG2 and Huh7 cells were seeded at a density of 8×10^3 cells/well in 96-well plates and maintained for 72 h at 37°C , 5% CO_2 and 95% humidity until they were treated with $0.6 \mu\text{M}$ broxbam or $2.0 \mu\text{M}$ vorinostat for 3, 6 and 18 h at 37°C , 5% CO_2 and 95% humidity. To measure MMP, cells were stained for 15 min in the dark at 37°C using the JC-1 dye (1 mg/ml; 5,5',6,6'-tetrachloro-1,1',3,3'-tetraethylbenzimidazolylcarbocyanine iodide; Molecular Probes; Thermo Fisher Scientific, Inc.). The cells were analysed using a Varioskan Flash fluorometer (Thermo Fisher Scientific, Inc.) at excitation wavelengths of 485 nm and emission wavelengths of 535 nm. Signals in the orange region of the fluorescence can be detected when JC-1 aggregates occur because of a negative MMP, which indicates healthy mitochondria. In the event of a positive MMP, which results from mitochondrial damage, JC-1 occurs in its monomeric form giving rise to fluorescence in

the green wavelength region (38). Accordingly, measurement of the ratio of orange to green fluorescence signal intensities allows the determination of changes in the MMP.

Western blotting. Whole cell extracts were prepared after harvesting substance-treated cells. HepG2 and Huh7 cells were incubated (37°C , 5% CO_2 and 95% humidity) for 24 h in RPMI growth medium (Gibco; Thermo Fisher Scientific, Inc.) containing the respective concentrations of test compounds (BB: 0.6 and $1.2 \mu\text{M}$; Vs, $4.0 \mu\text{M}$). Lysis was performed by using lysis buffer (0.1% SDS, 0.5% sodium deoxycholic acid, 1% Nonidet P-40, 0.1 mM PMSF, 1 mg/ml aprotinin and 1 mg/ml pepstatin A1; all from Sigma Aldrich; Merck KGaA). Protein contents of samples were determined using a BCA protein assay kit and samples containing 30 μg protein subjected to 7.5% or 12% SDS-PAGE. Proteins were then transferred onto PVDF membranes by electroblotting for 1.5 h. Membranes were blocked for 1 h using 5% skimmed milk powder solution followed by incubation at 4°C overnight with primary antibodies. The following antibodies were used: Glucose transporter (GLUT) 2 (1:1,000; cat. no. 071402 MilliporeSigma), p53 and phosphorylated (p-) p53 (1:1,000; cat. nos. 9282 and 9286, respectively; Cell Signalling Technology, Inc.), HDAC1, HDAC2, HDAC4 and HDAC6 (1:1,000; cat. nos. 5356, 5113, 7628 and 7558, respectively; Cell Signalling Technology, Inc.). Detection of tubulin (anti-Tubb2B, cat. no. TA337744; Origene Technologies, Inc.) served as a loading control. Membranes were washed with 0.1% Tween in PBS and incubated with HRP-coupled anti-IgG antibody (1:10,000; cat. nos. NA934 and NA931, Amersham; Cytiva) for 1 h at room temperature. Protein signals were visualised using enhanced chemiluminescent detection kit (Amersham; Cytiva) and a Fusion SL camera (Vilber Lourmat Deutschland GmbH). For quantification, ImageJ (Vs 1.53j, National Institutes of Health) was used and the density of the protein bands was normalised to tubulin as a loading control.

RT-qPCR. Cellular RNA of untreated HepG2 and Huh7 cells were extracted using GeneMATRIX Universal RNA Purification Kit (Roboklon GmbH) according to the manufacturers' protocols, followed by treatment with 1 U DNase I (Gibco; Thermo Fisher Scientific, Inc.) per μg RNA for the elimination of possible DNA contaminations. Reverse transcription into cDNA and qPCR were performed using GoTaq[®] 1-Step RT-qPCR System (Promega Corporation) on a QuantStudio 5 Real-Time PCR System (Thermo Fisher Scientific, Inc.). The mixture for each sample/primer mix had a final volume of $10 \mu\text{l}$ containing 20 ng RNA and 250 nM of each primer. Melt curve controls were run to ensure primer specificity. The parameters for reverse transcription were as follows: 37°C for 15 min, 95°C for 10 min. Primer sequences are listed in Table SI. The obtained cDNA was analysed by using GoTaq[®] 1-Step RT-qPCR System (Promega Corporation) and qPCR was run on a StepOne-Cycler (Thermo Fisher Scientific, Inc.) for 40 cycles of amplification (initial denaturation for 5 min at 95°C ; followed by denaturation at 95°C for 15 sec, annealing at 60°C for 20 sec, elongation at 72°C for 45 sec for 40 cycles). All samples were run in triplicate. The relative target gene expression was calculated using the $2^{-\Delta\Delta\text{C}_q}$ method using GAPDH, β -actin or 18S rRNA as an internal control (39).

Inhibition of HDAC activity. The ability of broxbam to inhibit HDAC1, -2, -4 and was measured using a cell free fluorogenic HDAC Assay (cat. nos. 50061, 50062, 50064, 50076 BPS Bioscience, Inc.). The HDAC activity was measured according to the protocols of the manufacturer. Briefly, purified human recombinant HDAC enzymes contained with the assay kit and fluorogenic HDAC substrates were used to measure HDAC activity. In total, 50 μ l assay buffer containing 1 μ g/ μ l BSA, the human recombinant HDAC enzyme, the test compound and the corresponding HDAC substrate was added into a black 96-well assay plate. The reaction in each well was incubated at 37°C for 30 min, followed by the addition of 50 μ l HDAC developer reagent and incubation at room temperature for 15 min. Fluorescence intensity was measured using a Varioskan Flash Fluorometer (Thermo Fisher Scientific, Inc.) using an excitation wavelength of 380 nm and an emission wavelength of 460 nm.

Immunofluorescence staining of the cytoskeleton. HepG2 cells were seeded onto glass coverslips at a density of 1×10^5 and were allowed to attach and proliferate for 24 h (37°C, 5% CO₂ and 95% humidity). Cells were treated with broxbam (0.6 μ M) and vorinostat (4 μ M) whereas a corresponding volume of DMSO was used as a negative control. Treated cells were incubated for additional 24 h (37°C, 5% CO₂ and 95% humidity) and fixed with 4% formaldehyde in PBS for 20 min at room temperature. The samples were then blocked and permeabilised (1% BSA and 0.1% Triton X-100 in PBS) for 30 min at room temperature. For the immunostaining of the microtubule structures, the cells were incubated for 1 h at 37°C in the dark with mouse primary anti-human α -tubulin monoclonal antibody (1:500; cat. no. T6199; Sigma Aldrich; Merck KGaA), followed by treatment with a AlexaFluor[®]-conjugated 546 goat anti-mouse secondary antibody (1:500; cat. no. A-21133; Thermo Fisher Scientific, Inc.) for 1 h at room temperature in the dark. Cellular actin filaments were stained for 1 h at 37°C in the dark using phalloidin (1:1,000, cat. No. A12379 AlexaFluor[®]-conjugated 488; Invitrogen; Thermo Fisher Scientific, Inc.). Coverslips were mounted in DAPI containing Mowiol (Mowiol 4-88; 1 μ g/ml DAPI; Carl Roth GmbH) for additional nuclei counterstaining. Fluorescence microscopic imaging (magnification, x60; Spinning Disk Confocal microscope; Nikon Corporation) was performed at the Charité Advanced Medical BioImaging Core Facility (Berlin, Germany).

Scratch wound healing assay. HepG2 cells were allowed to proliferate to confluence in six-well plates. Using a 10 μ l pipette tip, the cell monolayer was scratched once horizontally and vertically. Wells were rinsed with PBS and fresh medium was added, containing two concentrations of broxbam (0.6 and 1.2 μ M), whereas a corresponding volume of DMSO was used for a control. The cell monolayers were incubated for 24 h (37°C, 5% CO₂ and 95% humidity), followed by photographic documentation using a digital camera (Kappa Optonics GmbH). Migration of cells was quantified using the TScratch software (version 1.0; CSElab). Migration values were normalised to control, which was set as 100%. The experiments were performed under normal FBS conditions (10%), since HepG2 cells could not tolerate serum deprivation

and reacted with immediate and pronounced cell detachment. In addition, serum deprivation is a procedure that is preferable necessary for long-term observations (>24-48 h), where cell proliferation instead of migration becomes the predominant factor for wound healing (40,41).

Zebrafish angiogenesis assay. To examine the angiogenesis *in vivo*, experiments with zebrafish embryos were performed, which represents a viable model for the evaluation of angiogenic effects of small molecules (42). In the developing zebrafish embryo, the sub-intestinal veins (SIVs) represent a characteristic blood vessel system that can be easily visualised (42). Eggs from the transgenic Tg(fli1:EGFP)^{y1} mutant Casper zebrafish stem were obtained 2-5 h after egg deposition connected to spawning process from the animal breeding facility of the University of Bayreuth, which has the permission to keep and breed vertebrates and cephalopods for experimental purposes according to § 11 German animal Welfare Law (permission no. OBK/A 2; Bayreuth, Germany). Zebrafish are kept at 20-26°C in water pH 6.0-8.0 under standard atmosphere.

After the egg deposition, the spawn fish eggs (1 day post fertilisation) were collected, rinsed, and transferred into a petri dish filled with E3-medium (5 mM NaCl, 0.17 mM KCl, 0.33 mM CaCl₂, 0.33 mM MgSO₄ and 0.01% methylene blue in ddH₂O; pH 7.2) and incubated for 24 h at 28°C. Healthy embryos were then dechorionated, which means the removal of the egg shell, and five embryos per well were transferred into six-well plates in 5 ml E3-medium. In total, 100-fold pre-dilutions of test compounds (final concentrations were 1 μ M, 750 and 500 nM) in ddH₂O were prepared and added to the E3-medium at 50.5 μ l per well, followed by incubation for 48 h at 28°C. After the addition of 50 μ l 0.04% tricaine solution (ethyl-3-aminobenzoate-methanesulfonate; Sigma Aldrich; Merck KGaA) to the E3-medium in the six-well plates, the embryos (3 days post fertilisation) were anaesthetised (5 min at room temperature) to a final tricaine concentration of 0.0004% before the blood vessel system was visualised and documented by fluorescence microscopy with up to two-fold magnification (excitation wavelength, 488 nm; emission wavelength, 510 nm; Leica MZI0F fluorescence microscope; Leica Microsystems GmbH; AxioCam 1 cm; Carl Zeiss AG). The area of SIVs was measured using Image J version 1.52a. At the end of the experiments, 1 ml anaesthetic tricaine (tricaine mesylate; 5 g/l) was added to 5 ml E3-media to kill the zebrafish larvae (3 days post fertilisation) with an overdose of the anaesthetic, at a final concentration of 833 mg/l.

Statistical analysis. Statistical analysis of the data was performed using GraphPad Prism 8 software for Windows (GraphPad Software, Inc.). If not indicated otherwise, data were presented as the mean \pm standard error of the mean. Unpaired Student's t-tests were used for two-group comparisons. To test for statistical significance between > two groups, one-way ANOVA coupled with Tukey's post hoc tests was used. P<0.05 were considered to indicate a statistically significant difference. All experiments were performed in triplicate unless otherwise stated. The exact number of independent repetitions for each assay is provided in the figure legends.

Table I. Growth inhibitory concentrations (IC₅₀) of compounds applied to liver cancer cell lines HepG2 and Huh7, CCC cell lines TFK-1 and EGI-1 and mouse hepatocytes (AML12)^a.

Origin	Cell line	Broxbam (μM)	Vorinostat (μM)
Liver cancer	HepG2	0.6±0.2	2.1±0.4
	Huh7	0.6±0.1	1.8±0.5
CCC	TFK-1	0.6±0.1	1.4±0.1
	EGI-1	0.6±0.2	3.2±0.1
Non-transformed mouse hepatocytes	AML12	1.9±0.2	1.7±0.2

^aValues are derived from dose-response curves obtained by measuring the percentage of vital cells relative to untreated controls 48 h after incubation using crystal violet staining. Results are shown as mean \pm SD from $n \geq 3$ independent experiments. CCC, human cholangiocellular carcinoma.

Results

Inhibition of cell proliferation and cytotoxicity. It was previously reported that broxbam exerts selective anti-tumour effects at half maximal inhibitory concentrations (IC₅₀) in the low μM to two-digit nM range (20). In the present study, the potential effects of broxbam in liver cancer cell models were evaluated. Table I summarises the IC₅₀ values calculated for broxbam and vorinostat in liver cancer cell lines HCC and CCC and non-transformed hepatocytes. Notably, broxbam exhibited higher antiproliferative potency in all liver cancer cell lines compared with non-transformed hepatocytes, which required three-times higher IC₅₀ concentrations (Table I). This suggests the selectivity of broxbam towards liver cancer cells. In addition, broxbam exerted higher antiproliferative capabilities compared with the clinically relevant HDACi vorinostat in all liver cancer cell models test. Unlike broxbam, vorinostat did not appear to display cancer specificity, since its IC₅₀ values did not differ between the liver cancer cell lines and the non-transformed AML-12 cells (Table I).

Using the iCELLigence real-time cell viability and proliferation analysis system, the kinetic profile and onset of the inhibition of proliferation mediated by broxbam were determined. In case of the HepG2 and Huh7 cell lines, a distinct reduction in cell proliferation was observed at as early as 12 h after the application of broxbam in a dose-dependent manner (Fig. 2A and B). In CCC cell lines, this dose-dependent inhibitory effect was also detected, but instead becoming more pronounced 24 h after treatment (Fig. 2C and D). To exclude the contribution of unspecific cytotoxicity to these antiproliferative effects exerted by broxbam, the release of lactate dehydrogenase (LDH) from the cytosol into the cell culture supernatant of HepG2, Huh7 and AML12 cells was measured (Fig. 3). Increased LDH release would indicate the presence of nonspecific and necrotic cell death due to treatment-induced damage of cell membranes (36). However, treatment of HepG2 or Huh7 cells with rising concentrations of broxbam (0.1-10 μM) did not lead to significant increases in LDH release after 24 h (Fig. 3). The same effects were also observed in non-transformed hepatocytes (AML12) after broxbam treatment (Fig. 3). This suggests that broxbam does not compromise cell membrane integrity and that it exerted no

immediate cytotoxic effects even at concentrations as high as 10 μM .

In vivo tumour growth reduction. The potential antineoplastic effects of broxbam in liver cancer tumours was next tested using *in vivo* chick embryo experiments, specifically by applying the modified chorioallantoic membrane (CAM) assay. HepG2-derived microtumours from an initial volume of 20 μl were grown on the CAM of fertilised chicken eggs for 24 h. Subsequently, the microtumours were treated for 72 h with either PBS (control) or rising concentrations of broxbam (1.2-5.0 μM). At the end of the experiment, tumour masses were excised and weighed. Compared to PBS-treated controls, broxbam (3 and 5 μM) induced a significant reduction in liver cancer microtumour growth (Fig. 4).

To further characterise the underlying signalling and metabolic events underlying these antitumor effects of broxbam observed in the present study, its potential effects on glucose metabolism were next assessed. Cancer cells preferentially use glycolysis to consume glucose as the substrate for energy metabolism, in a process known as the Warburg effect (43). Therefore, the impact of broxbam on the expression of GLUT2, which is crucial for hepatic glucose uptake (44), was investigated. In addition, the glycolytic activity of HepG2 and Huh7 cells was also assessed by measuring the consumption of glucose, production of lactate and its release into the supernatant of the cell culture medium. Protein expression levels of GLUT2 were not affected by broxbam, though the HDACi vorinostat markedly reduced the expression of GLUT2 compared to broxbam treated group in both HepG2 and Huh7 cells (Fig. S1). This finding suggests that vorinostat, but not broxbam, can inhibit cellular glucose uptake by downregulating GLUT2 expression. By contrast, the glycolytic activity of broxbam-treated liver cancer cells was found to be decreased significantly. Compared with that in the untreated controls, the remaining glucose in the cell culture supernatant of broxbam-treated HepG2 cells was markedly higher whereas the production and release of lactate was decreased (Fig. S1). This lower glucose consumption and reduced lactate production indicate reduced glycolytic activity in broxbam-treated cells. In addition, no such reduction in glycolytic activity could be observed in HepG2 cells

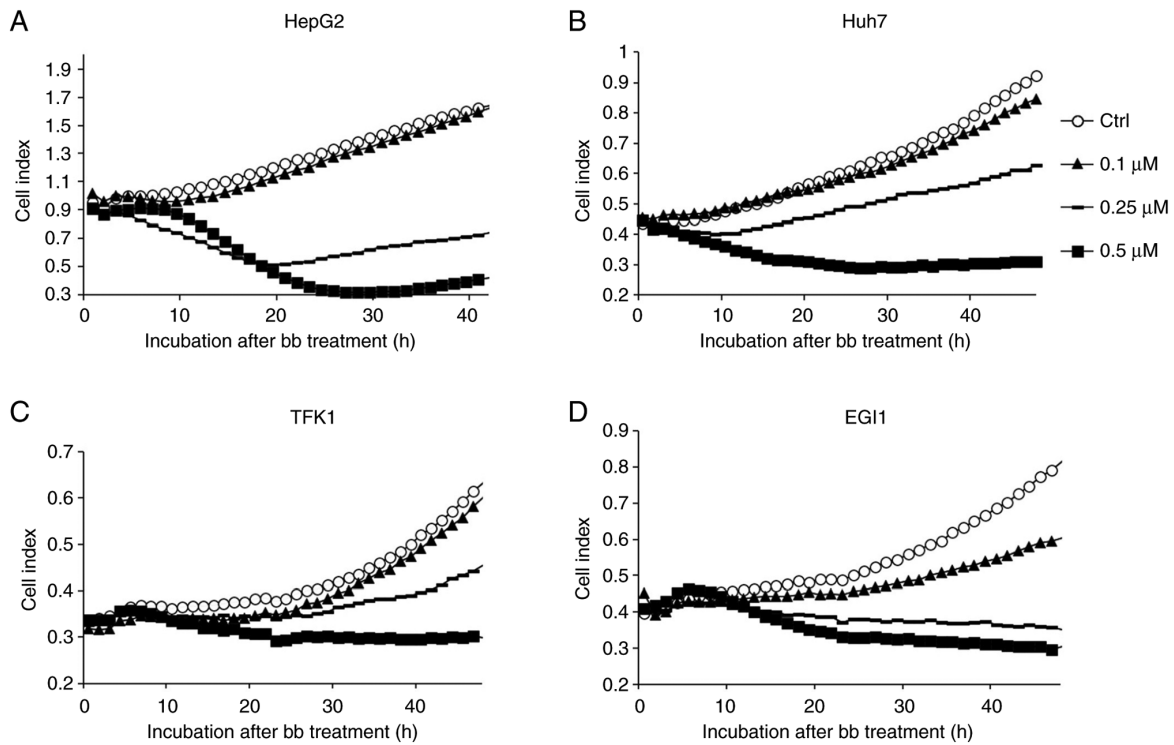


Figure 2. Real-time measurements of liver cancer and cholangiocellular carcinoma cell proliferation. Dose- and time-dependent effects of bb on (A) HepG2, (B) Huh7, (C) TFK1 and (D) EGI1 cell proliferation as assessed by the iCELLigence real-time monitoring system. Data show the cell viability index measured over 48 h after the application of broxam. Representative graphs out of three independent experiments were shown for each cell line. Bb, broxam.

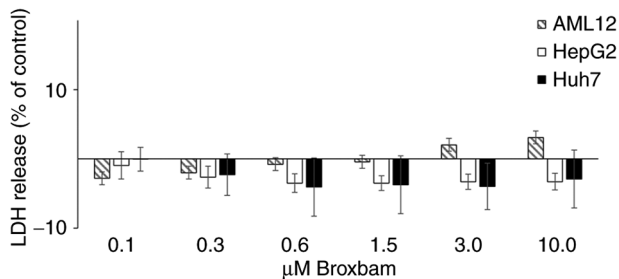


Figure 3. LDH release by liver cancer cell lines HepG2 and Huh7 and the non-transformed hepatocyte cell line AML12 into the media after 24 h treatment with broxam in different concentrations. Data are presented as the LDH release relative to those in untreated controls, where basal LDH release was set to 0%. Values are presented as the mean \pm SEM. n=4. LDH, lactate dehydrogenase; ctrl, control.

following vorinostat treatment, suggesting no effects were mediated by vorinostat on glucose uptake or lactate production and release.

Proapoptotic mode of action. To further elucidate the mechanisms by which broxam exerted antitumour effects on the liver cancer cells the extent of apoptosis induction was next measured. Apoptosis induction considered to be one of the primary objectives of targeted cancer therapy since it results in the specific and inflammation-free elimination of cancer cells. Apoptosis induction occurs through two distinct mechanisms, either by the activation of cellular death receptors or through the mitochondria-driven activation of caspase-3 (45). Broxam was found to induce mitochondria-driven apoptosis in liver cancer cells, as evidenced by fluorometric changes in the

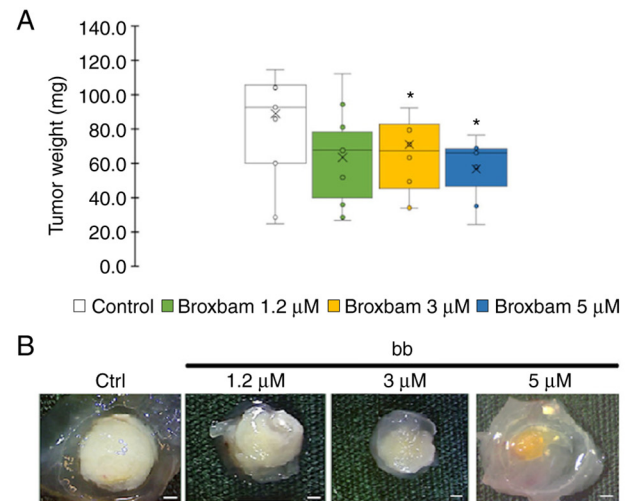


Figure 4. Measurement of tumour size grown on the chorioallantoic membranes of fertilised chicken eggs. (A) Tumour mass of HepG2 tumours after treatment with different concentrations of bb and PBS as control for 72 h. Data are presented as the mean \pm SEM from seven independent experiments. *P<0.05. (B) Representative images of control and bb-treated HepG2 tumours after excision. Scale bar 800 μ m. bb, broxam; Ctrl, control.

MMP of broxam treated cells (Fig. 5A). An increase in the green/red ratio indicates a reduction in the MMP and therefore mitochondrial damage, which may have served as a trigger for the activation of the apoptosis-associated tumour suppressor protein p53. A significant increase in the green/red ratio following treatment with the IC₅₀ concentration of broxam at 0.6 μ M was observed after 3 and 6 h (Fig. 5A).

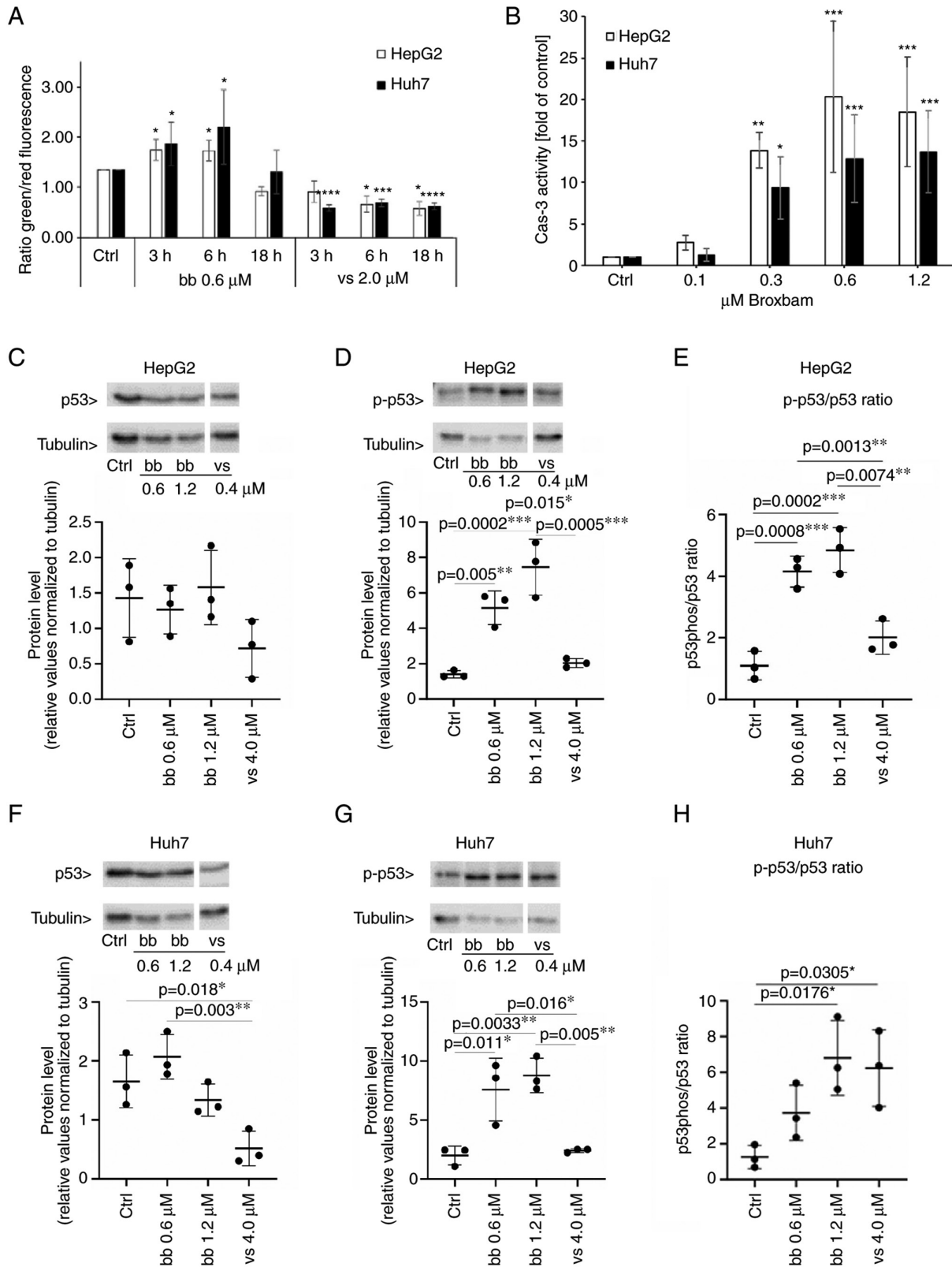


Figure 5. Detection of proapoptotic events in liver cancer cells. (A) Influence of bb and vs on the loss of mitochondrial membrane potential of liver cancer cell lines HepG2 and Huh7. Indicated values were measured by fluorometric measurement of JC-1-stained cells. The effect of IC₅₀ concentrations of bb and vs was monitored after 3, 6 and 18 h. Mitochondrial accumulation of JC-1 results in red fluorescence whereas loss of MMP results in monomeric JC-1, which emits green fluorescence. Data are presented as the ratio of green/red fluorescence of cells. Data are presented as the mean \pm SEM from three experiments. One-way ANOVA with Tukey's post hoc test was used to test for significance. *P<0.05, ***P<0.001 and ****P<0.0001 vs. Ctrl. (B) Caspase-3 activity in HepG2 and Huh7 cells upon treatment with bb for 24 h. Data are presented as the mean \pm SEM percentage of untreated controls from four experiments. One-way ANOVA with Tukey's post hoc test was used to test for significance. *P<0.05, **P<0.01 and ***P<0.001 vs. ctrl. (C-H) HepG2 and Huh7 cells were treated either with solvent (Ctrl), bb at IC₅₀ (0.6 μ M), bb at two-fold IC₅₀ (1.2 μ M) or vs. at two-fold IC₅₀ (4.0 μ M). Western blotting results of (C) p53 expression and (D) phosphorylation levels in HepG2 cells. (E) p-p53/p53 ratio was also quantified in HepG2 cells. Western blotting results of (F) p53 expression and (G) phosphorylation levels in Huh7 cells. (H) p-p53/p53 ratio was also quantified in Huh7 cells. Corresponding representative western blotting images are shown in Fig. S2. n=3 per group. One-way ANOVA with Tukey's post hoc test was used to test for significance. Bb, broxbam; vs, vorinostat; Ctrl, control; Cas 3, caspase 3; p-, phosphorylated.

By contrast, treatment with vorinostat at its IC_{50} concentration of $2 \mu M$, did not lead to an apoptosis-inducing increase in the green/red ratio. Instead, a significant reduction was observed, suggesting that vorinostat was not likely to induce mitochondria-driven apoptosis (Fig. 5A).

In following experiments broxbam treatment was shown to induce a dose-dependent increase in the phosphorylation of p53 of HepG2 and Huh7 cells (Fig. 5C-H), consistent with the aforementioned data on the broxbam-induced changes in MMP for the initiation of mitochondria-driven apoptosis (Fig. 5A). In addition, no increase in p53 phosphorylation in HepG2 (Fig. 5D) or Huh7 (Fig. 5G) cells could be observed after vorinostat treatment, which is in accordance with the failure of vorinostat to decrease the MMP (Fig. 5A).

Mitochondria serve a pivotal role in the regulation of apoptotic caspase activation. The caspase cascade lies downstream of the loss of MMP and activation of p53 (46-48). This cascade eventually leads to the activation of the executioner caspase-3 (49). Therefore, Caspase-3 activity was next assessed using a fluorogenic caspase-3 assay, which functions by the specific recognition of the enzymatic activity of phosphorylated caspase-3 (15). After broxbam treatment, HepG2 and Huh7 cells exhibited a dose-dependent increase in apoptotic caspase-3 activity compared with that in the control group (Fig. 5B). Of note, maximal caspase-3 activity could already be observed at the concentration of $0.6 \mu M$ broxbam (Fig. 5B), which corresponded to the IC_{50} values of broxbam in these cells (Table I).

HDAC expression and activity. To clarify if HDAC inhibition forms part of the antitumour mechanism of broxbam, its effects on HDAC expression and activity were investigated. RT-qPCR was used to measure the expression levels of the 11 subtypes of HDACs (HDACs 1-11) in the HepG2 and Huh7 cells. Although the mRNA expression levels of HDAC1 and HDAC2 were considerably lower compared with those of the other HDAC subtypes, all 11 HDACs tested were found to be expressed in both cell lines (Fig. 6).

Subsequently, the potential treatment-induced changes in the protein expression levels of HDAC1, -2, -4 and -6 were assessed by western blotting and densitometric analysis. HDAC1 and HDAC2 belongs to class I HDACs and are localized in the nucleus of the cell (50). HDAC4 and HDAC6 are class II HDACs and both can be found in the cytoplasm as well as in the nucleus of a cell (50). These HDACs were previously found to be overexpressed in human pancreatic adenocarcinoma and hepatocellular carcinoma (50,51). Exposure of HepG2 and Huh7 cells to $0.6 \mu M$ and $1.2 \mu M$ broxbam, concentrations corresponding to their respective IC_{50} and two-fold IC_{50} values, did not lead to significant changes in any of the HDAC subtypes (Fig. 7). An exception was the significant increase in HDAC4 expression in Huh7 cells treated with $1.2 \mu M$ broxbam compared with that in the control group (Fig. 7C). This finding suggests that broxbam functions as an inhibitor of HDAC activity instead of being a regulator of HDAC expression (Fig. 7).

The activities of HDACs -1, -2, -4 and -6 following treatment with IC_{50} and two-fold IC_{50} concentrations of broxbam and vorinostat were assessed using a cell-free enzymatic assay system. HDAC subtype-specific inhibition of the cleavage of

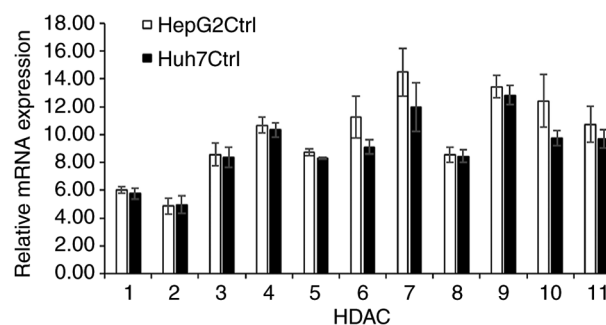


Figure 6. mRNA expression levels of HDACs 1-11 in untreated liver cancer cell lines HepG2 and Huh7. mRNA expression levels of HDACs 1-11 in liver cancer cell lines were measured using reverse transcription-quantitative PCR, which were then normalised to those of GAPDH, the housekeeping gene. Data are presented as the means \pm SEM from three independent experiments. HDAC, histone deacetylase; Ctrl, control.

fluorogenic peptide substrates (Fig. 8A) was next detected and compared with the untreated control group, which was set to 100%. Broxbam exerted an attenuating effect on the activity of HDAC1 and -6, but did not affect the activities of HDACs -2 and -4. Vorinostat mediated potent inhibitory effects on the HDACs -1 and -2, which exceeded that of broxbam. Therefore, broxbam and vorinostat inhibited the individual HDAC isoforms with distinct profiles. However, both compounds were concluded inhibit HDAC1, with broxbam showing specificity towards HDAC6 whereas vorinostat showed specificity towards HDAC2. Due to this potent inhibitory effect of broxbam against HDAC6, the present study next examined its potential dose dependency over the concentration range from 0.6 to $10 \mu M$, which revealed 90% inhibition of HDAC6 activity at $10 \mu M$, the highest broxbam concentration tested (Fig. 8B).

To investigate the contribution of HDAC6 inhibition towards the antiproliferative effects of broxbam in liver cancer cells (Fig. 2), HDAC6 knockdown was performed using siRNA. After 48 h of transfection with HDAC6-specific siRNA, the expression of HDAC6 protein in Huh7 cells was significantly decreased compared with that in cells transfected with the si-mock (Fig. 8C and D). Furthermore, the expression of typical markers of cell proliferation Ki-67 and E2F3 (52,53), were also found to be decreased significantly compared with that in cells transfected with the si-mock (Fig. 8E and F) suggesting a distinct contribution of HDAC6 inhibition towards the antiproliferative (Figs. 1 and 2) and antineoplastic (Fig. 4) effects of broxbam in liver cancer.

Dynamics of the cytoskeleton and cellular migration. Since broxbam contains the trimethoxystilbene motif of the vascular disrupting natural product CA-4 within its structure (23,25,26), it was next examined for its possible effects on the tubulin cytoskeleton and associated processes. Its inhibitory effects on the polymerisation of purified tubulin *in vitro* have already been previously reported (20). As HDAC6 has been found to function as a tubulin deacetylase to interfere with microtubule-dependent cell motility (54), the effects of broxbam on the microtubule and F-actin cytoskeleton of HepG2 cells were investigated using immunofluorescence staining. The formation of F-actin stress fibres and focal adhesions was observed

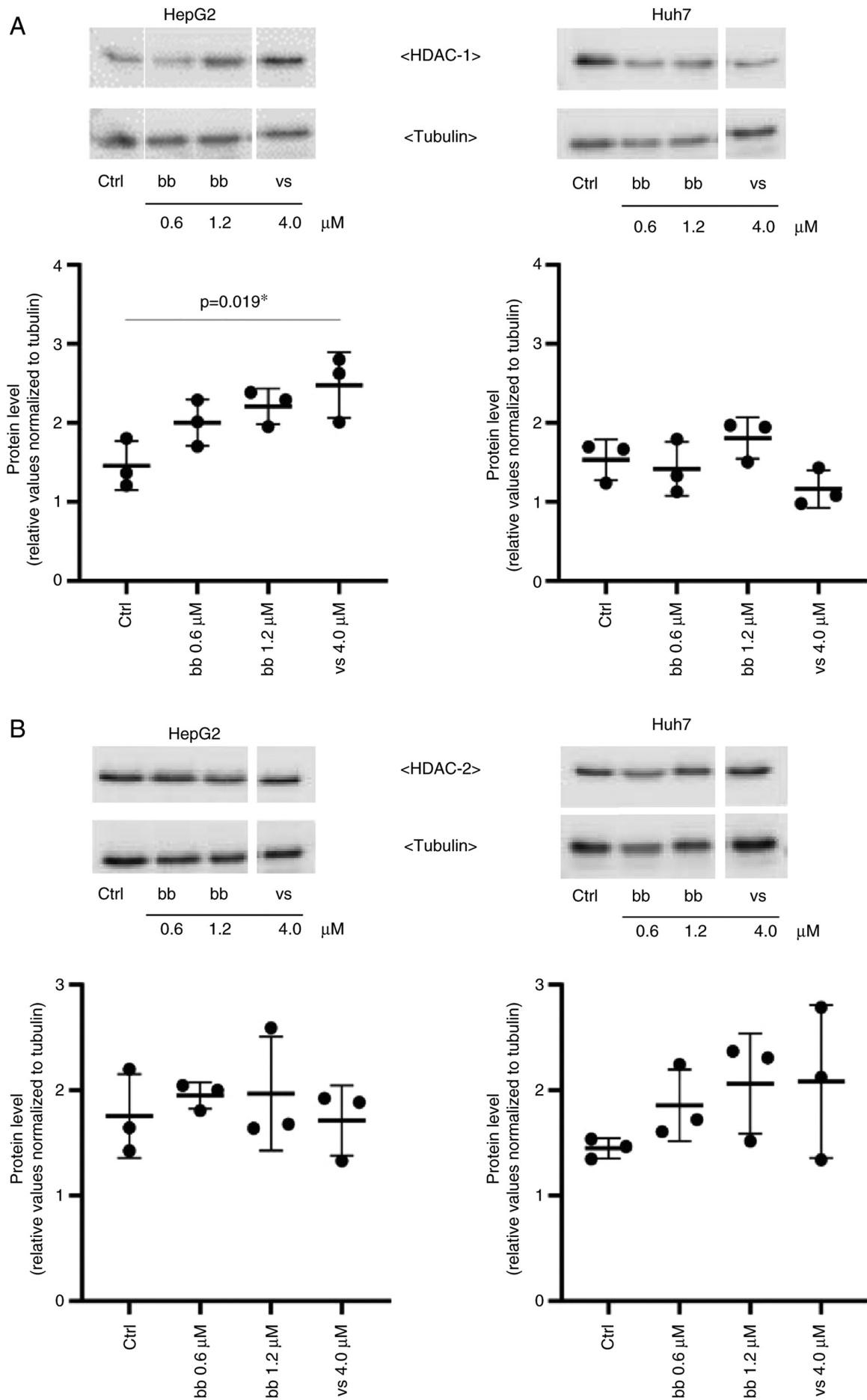


Figure 7. Continued.

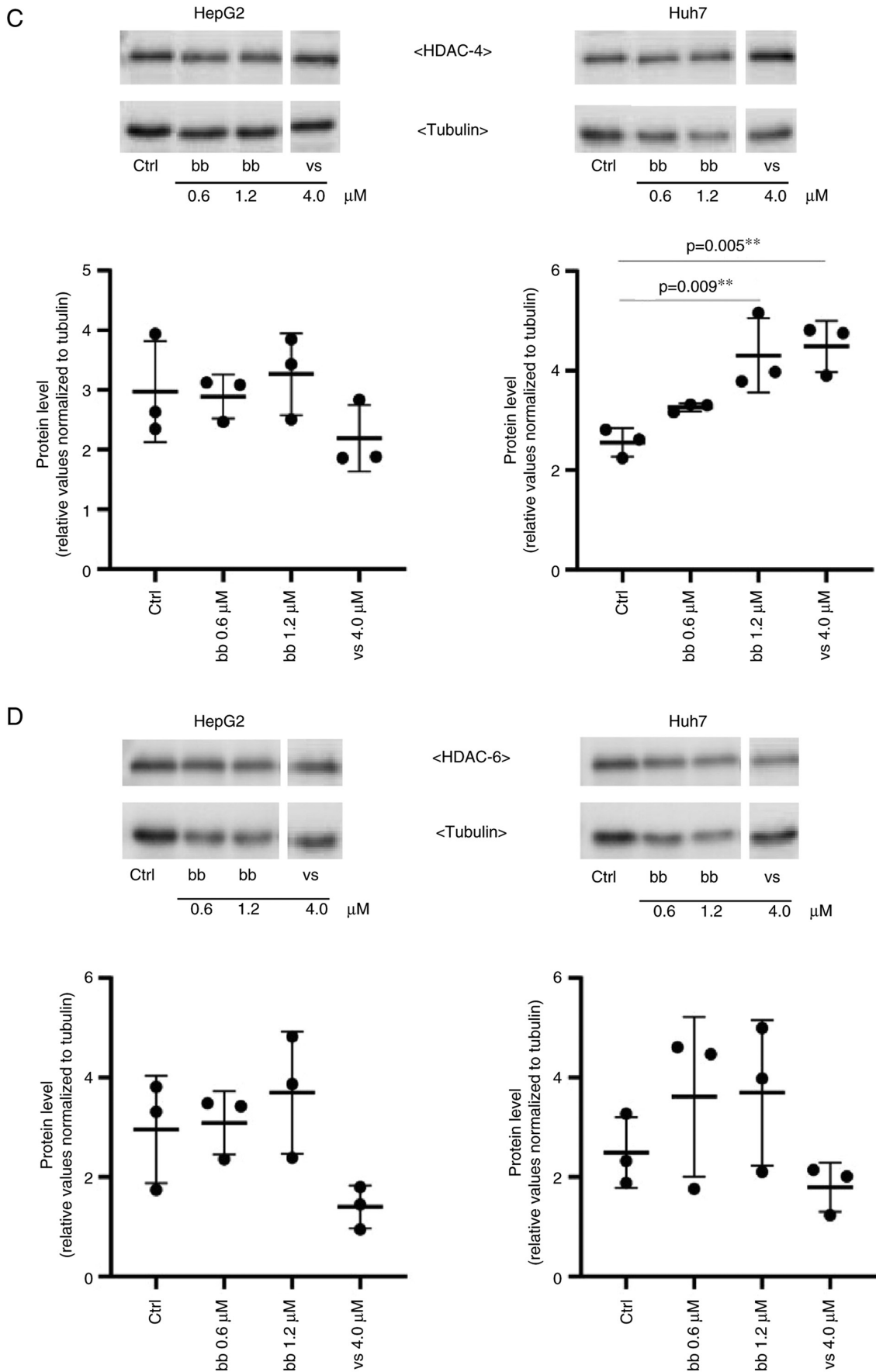


Figure 7. Quantification of the expression of selected HDAC proteins. HepG2 and Huh7 cells were treated for 24 h with either solvent (Ctrl), bb at IC_{50} ($0.6 \mu\text{M}$), bb at two-fold IC_{50} ($1.2 \mu\text{M}$) or vs. at two-fold IC_{50} ($4.0 \mu\text{M}$). Western blotting was used to measure protein expression, using tubulin as loading control. (A) HDAC1 expression in Hep2G and Huh7 cells. (B) HDAC2 expression in Hep2G and Huh7 cells. (C) HDAC4 expression in Hep2G and Huh7 cells. $^{**}P < 0.01$ vs. ctrl. (D) HDAC6 expression in Hep2G and Huh7 cells. Corresponding representative western blotting images are provided in Fig. S2. $n=3$ per group. One-way ANOVA with Tukey's post hoc test was used to test for significance. HDAC, histone deacetylase; Ctrl., control; bb, broxbam; vs, vorinostat.

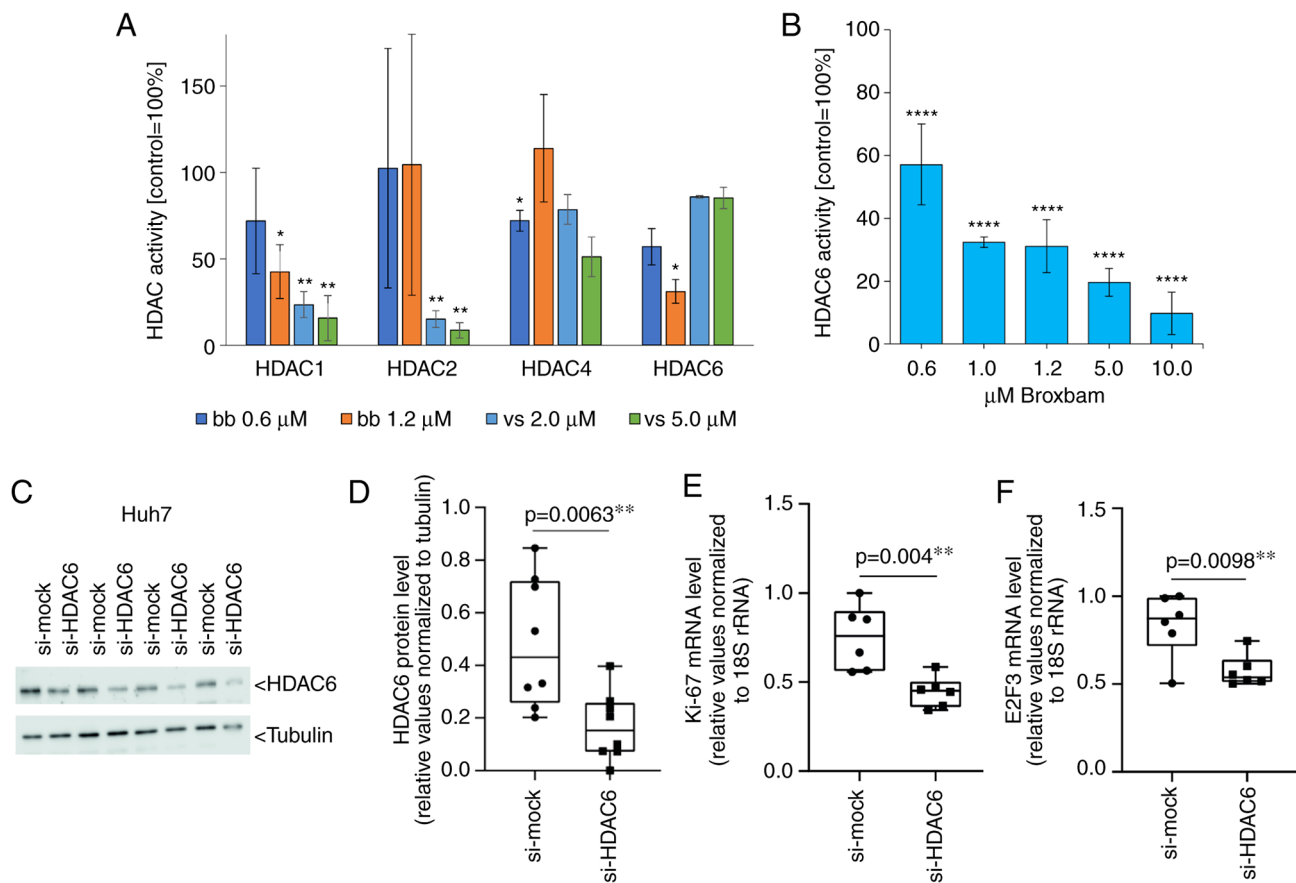


Figure 8. Effects of inhibiting the selective HDACs of broxbam in Huh-7 cells. (A) Activities of HDAC1, -2, -4 and -6 after treatment with bb or vs at concentrations corresponding to their respective IC_{50} and two-fold IC_{50} . Data are presented as the means \pm SEM percentage of untreated control, which was set to 100%, from three experiments. * $P<0.05$, ** $P<0.01$ vs. Ctrl. One-way ANOVA with Tukey's post hoc test was used to test for significance. (B) Dose-dependent inhibitory effect of bb on the activity of HDAC6 relative to control, represented as the means \pm SEM from three independent experiments. **** $P<0.0001$ vs. Ctrl. One-way ANOVA with Tukey's post hoc test was used to test for significance. (C) Western blot analysis and (D) quantification of siRNA-mediated knockdown of HDAC6 protein expression in Huh7 cells transfected with control (si-mock) or HDAC6-specific (si-HDAC6) siRNAs for 48 h. Each set of si-mock and si-HDAC6 lanes represents one transfection experiment. Tubulin was used as the loading control. Analysis of (E) Ki-67 and (F) E2F3 mRNA expression by reverse transcription-quantitative PCR. The mRNA expression levels were normalised to that of 18S rRNA. Data was presented as the mean \pm SEM from six independent experiments. One-way ANOVA with Tukey's post hoc test was used to test for significance. HDAC, histone deacetylase; bb, broxbam; vs, vorinostat; si, small interfering.

following treatment with broxbam at its IC_{50} concentration (Fig. 9). Furthermore, the microtubule cytoskeleton appeared to be markedly altered compared with that in the control group. In general, broxbam-treated cells were considerably enlarged, especially their nuclei (Fig. 9). These effects were more prominent compared with those mediated by vorinostat, even after treatment with vorinostat at a concentration of two-fold IC_{50} (Fig. 9).

Cytoskeletal components, such as microtubules and actin fibres, are critical for cell migration (55,56). To investigate the effect of broxbam on cell migration, a scratch wound healing assay was performed. An observation period of 24 h was chosen to minimise the possibility of the migratory process being distorted by cell proliferation. The average doubling time of HepG2 cells is ~ 48 h, suggesting that HepG2 cell proliferation is unlikely to contribute significantly to wound closing (57). Broxbam treatment led to a significant reduction in gap closing by the HepG2 cell monolayer compared with that in the untreated control group (Fig. 10). In addition, broxbam exerted a potent antimigratory effect even when applied at its IC_{50} concentration of 0.6μ M (Fig. 10B).

Antiangiogenic effects in vivo. A previous study validated the properties of the two structural motifs on broxbam, which are HDAC-inhibition mediated by the hydroxamic acid pharmacophore and interference with cytoskeletal dynamics by its trimethoxystilbene motif (20). There is a possibility that inhibition of tubulin polymerisation and HDAC activity by broxbam may also translate into an antiangiogenic effect. Due to the previously known antiangiogenic effects of CA-4 (23) and the well-established association between HDACs as modulators of hypoxia-induced factor-1 α and vascular endothelial growth factor (VEGF) expression (58), it was hypothesised that broxbam may also exert antiangiogenic properties. Therefore, *in vivo* zebrafish angiogenesis assays were performed (42). Broxbam mediated a dose-dependent antiangiogenic effect in reducing the area of the sub-intestinal veins (SIV) in developing zebrafish embryos, which became visible at concentrations equating to its IC_{50} value (Figs. 11 and 12). Signs of cardiotoxicity, such as dilation of the pericardial sac, which is a known unwanted side effect of antiangiogenic substances, such as CA-4 (59), could not be observed (Figs. 11 and 12).

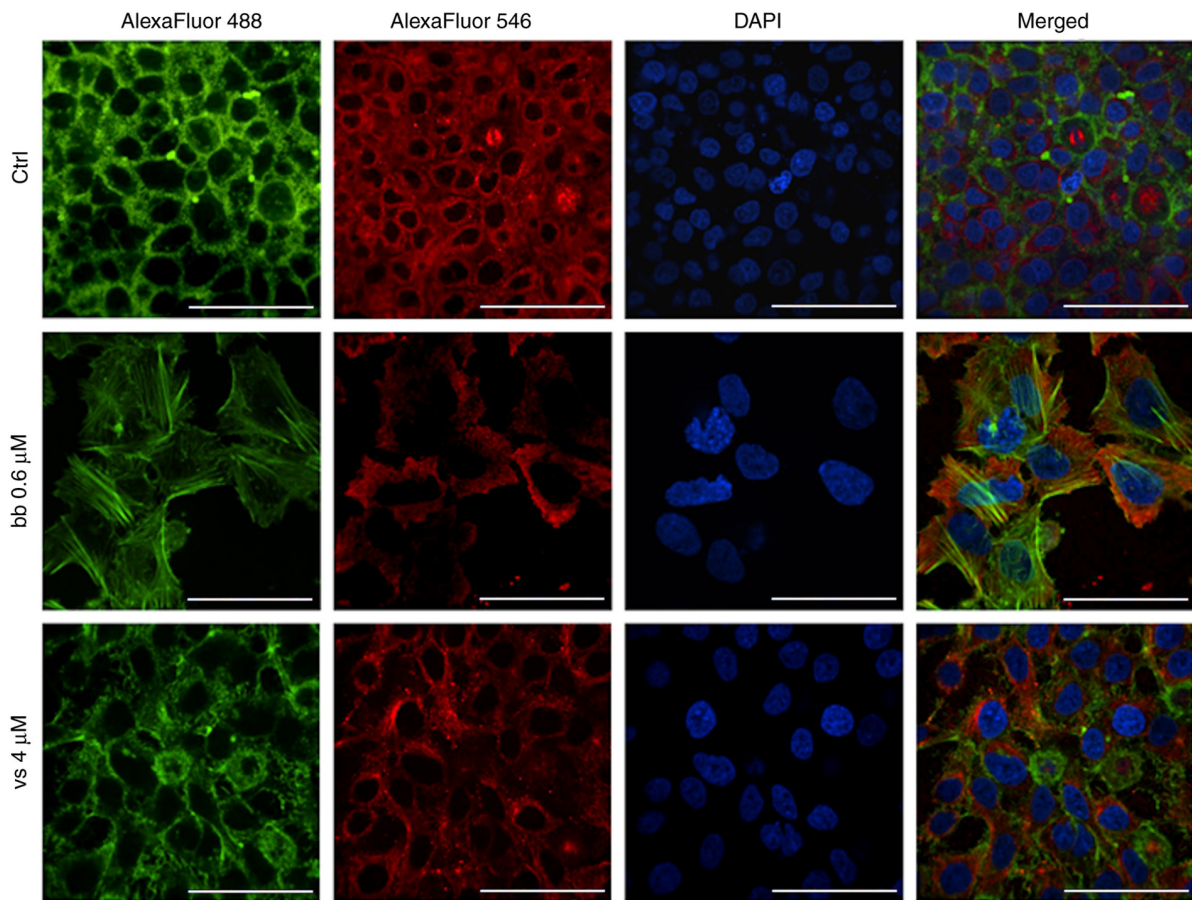


Figure 9. Responses of the cytoskeleton in HepG2 cells to bb treatment. Confocal immunofluorescence images 24 h after incubation with bb (0.6 μM) or vs. (4 μM). α -Tubulin (red), f-actin (green) and DAPI-stained nuclei (blue) staining are shown. Scale bar, 30 μm . Ctrl, control; bb, broxbam; vs, vorinostat. Images are representative of n=3 independent experiments.

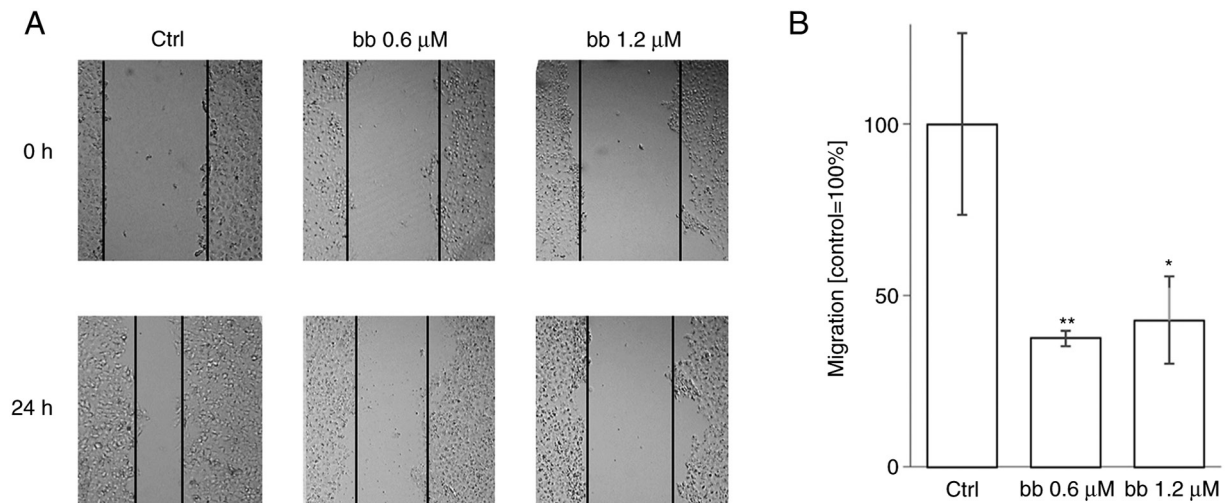


Figure 10. Effects of different concentrations of bb on the migration of HepG2 cells. HepG2 cell migration was measured using wound healing assays 24 h after treatment. (A) Representative images from five independent experiments, where the cells were treated with at IC_{50} two-fold IC_{50} of bb. (B) Cell migration was presented as the mean \pm SEM percentage of control from three experiments. One-way ANOVA with Tukey's post hoc test was used to test for significance. * $P < 0.05$ and ** $P < 0.01$ vs. ctrl. ctrl, control; bb, broxbam.

Discussion

Broxbam was recently reported to be a potent anticancer agent against various non-liver cancer cell models (20). In the

present study, it was shown to exert antiproliferative properties in HCC and CCC liver cancer cell models. This novel chimeric compound, which consists of a HDAC-inhibitory hydroxamic acid pharmacophore and a cytoskeleton-interfering

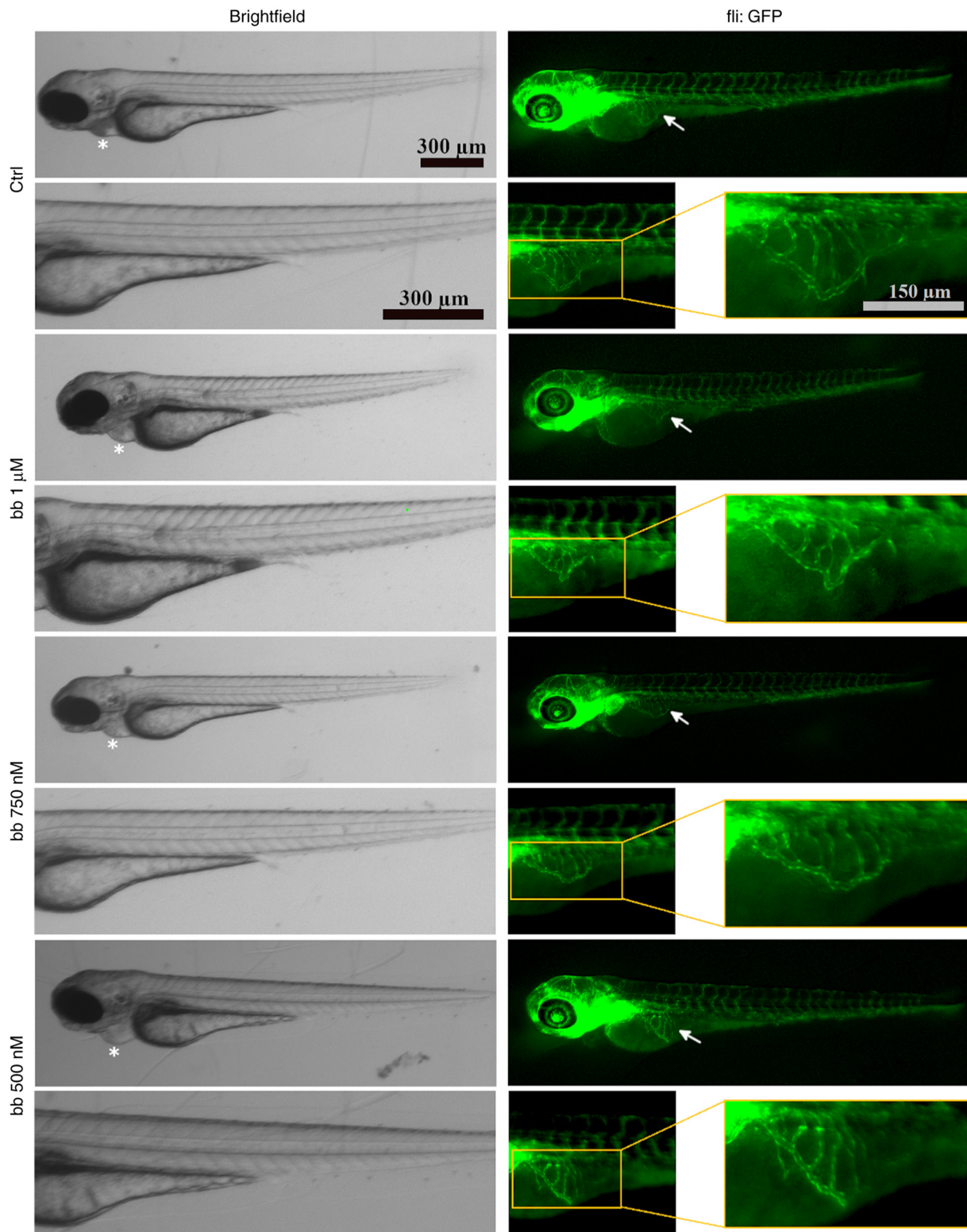


Figure 11. Morphology of the blood vessel system of transgenic $Tg(fli:EGFP)y1$ mutant Casper zebrafish embryos 72 h post-fertilisation. Embryos were treated for 48 h with either a corresponding amount of DMSO, with bb concentrations of 1 μM , 750 or 500 nM. Brightfield and green fluorescent images, denoted as fli:GFP, are shown. The pericardial region was marked with asterisks whereas SIVs are marked with arrows. Fluorescent SIV areas are marked with yellow boxes, which were then magnified two-fold magnification. Individuals shown are representative for ≥ 20 embryos per concentration. bb, broxbam; GFP, green fluorescent protein; SIV, sub-intestinal veins.

trimethoxystilbene motif, inhibited the proliferation of liver cancer cells at near-nanomolar concentrations (IC_{50} , $\sim 0.6 \mu M$). This exceeded the antiproliferative potency of the clinically established HDACi vorinostat (IC_{50} , 1.4-3.2 μM). Unlike

vorinostat, broxbam exerted preferential specificity for cancer cells over non-transformed murine hepatocytes. Real-time kinetic investigation of the antiproliferative effects of broxbam revealed an early onset of this effect, at 12-24 h, after drug

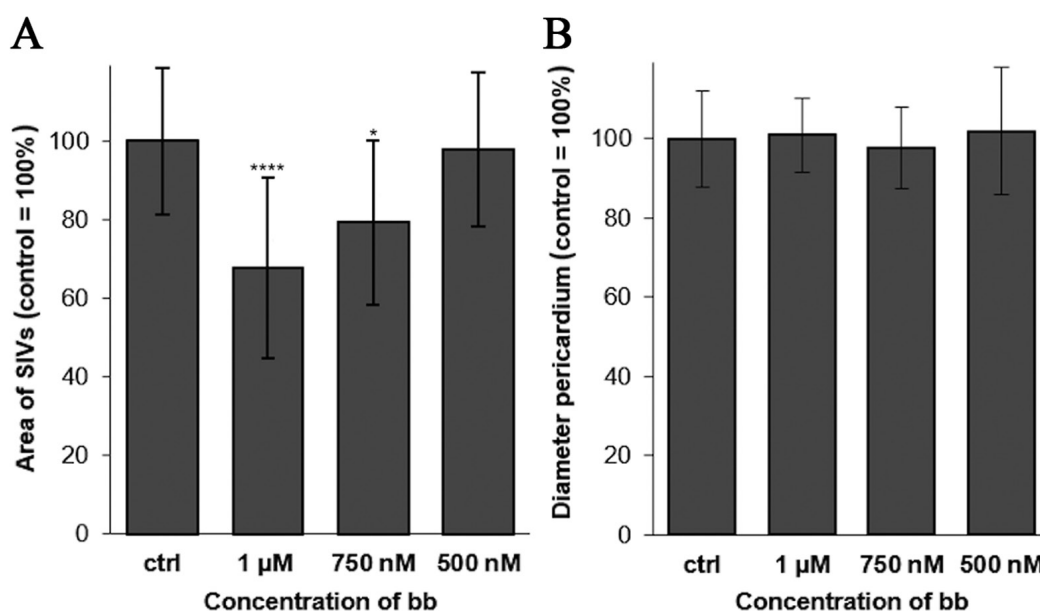


Figure 12. Effects of bb on developing zebrafish embryos at 3 days post fertilisation. (A) Area of SIVs after bb treatment with concentrations of 1 µM, 750 and 500 nM for 48 h. Values were normalised to the negative control, DMSO. (B) Percentage pericardial diameter relative to the negative control, DMSO. Data are presented as the percentage means \pm SEM of control from ≥ 20 experiments. Significance levels were determined using one-way ANOVA and Tukey's post hoc test. * $P < 0.05$ and **** $P < 0.0001$ vs. ctrl. bb, broxbam; SIV, sub-intestinal veins.

application. The prohibitive effects of broxbam on liver cancer cells was found not likely to be due to unspecific cytotoxicity, but instead likely to be due to the targeted and orchestrated modulation of cancer cell-specific signalling pathways. This in turn lead to antiproliferative, anti-angiogenic, anti-migratory and apoptotic effects, in addition to the breakdown of cellular energy metabolism. The decrease in the glycolytic activity of liver cancer cells after broxbam treatment may be of therapeutic importance in terms of the glucose addiction of cancer cells, which is required for the maintenance of metabolism (the Warburg effect) (43).

Broxbam was found to induce the apoptosis of liver cancer cells through the mitochondrial-driven apoptosis pathway. A protein of importance for mitochondrial apoptosis is the p53 tumour suppressor protein, the phosphorylation of which is associated with the disruption of mitochondrial function and subsequent cell death (48). Phosphorylation of p53 induces the expression of p53 regulated apoptosis inducing protein 1, which is localised in the mitochondria and leads to the disruption of MMP en route to triggering apoptosis (60,61). Consistent with this mechanism, the present study found that broxbam induced p53 phosphorylation, reduced MMP and subsequently activated the apoptosis-specific effector caspase-3. The activation of caspase-3 directly contributes to core apoptotic processes, such as the dismantling of cell components and formation of apoptotic bodies therefore, it represents a direct marker for the activation of apoptosis (62). The extent of apoptosis mediated by broxbam was studied in the present study in two liver cancer cell lines with distinct p53 statuses. HepG2 cells represents a p53-wild-type cell line whereas Huh7 cells harbour a mutated codon in the p53 gene leading to the overexpression of the functionally-repressed p53 (63). Caspase-3 activation by broxbam was more pronounced in the p53-native HepG2 cells compared with that in the p53-mutated Huh7 cells. However,

broxbam promoted p53 phosphorylation in both cell models without altering the expression of the total p53 protein. By contrast, vorinostat did not alter p53 phosphorylation in either of the cell models, whilst significantly downregulating p53 expression in Huh7 cells. It is tempting to speculate that this may be the result of differences in the HDAC subtype specificity between broxbam and vorinostat, especially in their inhibitory activities towards HDAC6 activity. However, further research is required to clarify this putative association. It is noteworthy that broxbam can induce p53 phosphorylation both in cells with wild-type and mutant p53, whilst vorinostat could not induce p53 phosphorylation.

Evaluation of the effects of broxbam and vorinostat on HDAC revealed that neither of the compounds significantly influenced the protein expression of the HDAC subtypes -1, -2, -4 and -6, instead inhibiting their HDAC enzyme activity. Subtype-specific profiling revealed pronounced differences in the ability of broxbam and vorinostat to inhibit HDAC6. Whilst broxbam potently inhibited HDAC6 activity (>90%) at a concentration of 10 µM, vorinostat could only mediate a comparatively weak inhibition of 20%.

HDAC6 is a unique member of the HDAC family not only for its role in histone acetylation and deacetylation, but also in targeting several non-histone substrates, such as cortactin and heat shock protein 90, thereby regulating cell proliferation, metastasis, invasion, and mitosis in tumours of SKOV3 human ovarian cancer cells (64). Accordingly, it has been previously demonstrated that HDAC6 inhibition can lead to the inhibition of cell proliferation, apoptosis, reduction in migration and motility of fibroblasts, SKOV3 ovarian cancer, SKBR3 breast carcinoma, and MCF7 breast cancer cell lines (65). This is consistent with observations in the present study with regards to the broxbam-mediated HDAC6 inhibition of liver cancer cells. HDAC6-specific siRNA silencing in Huh7 cells,

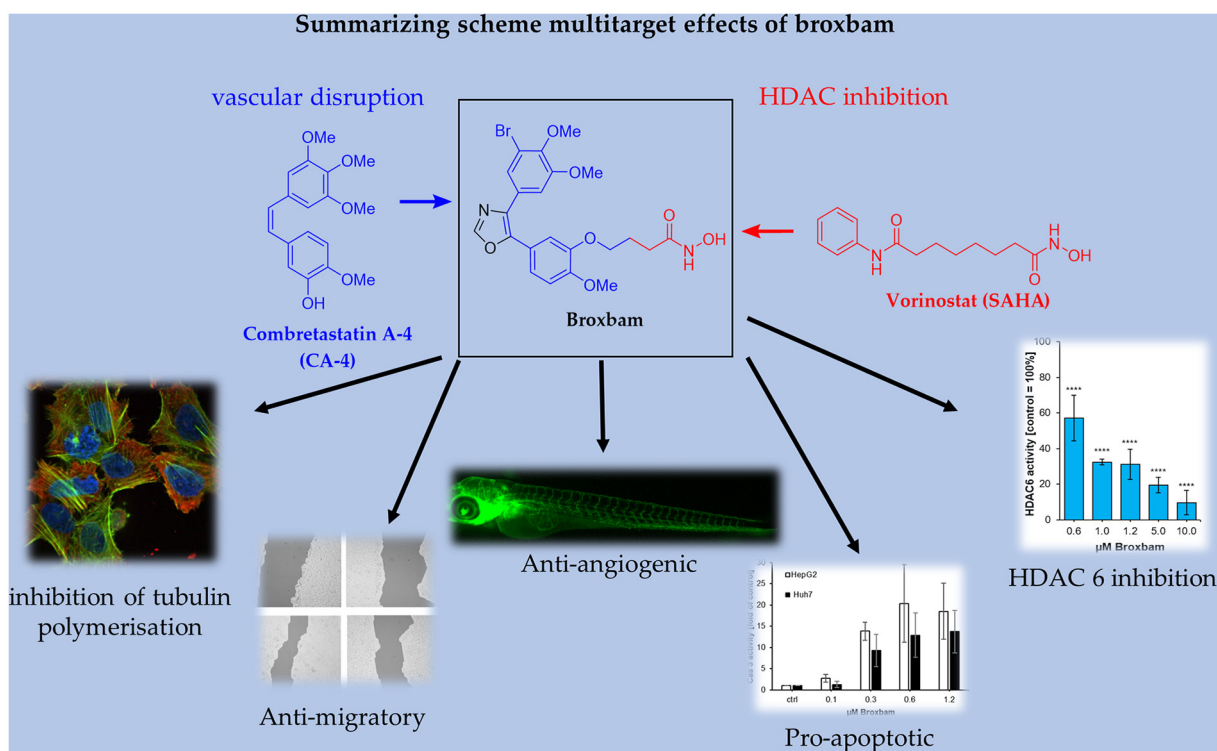


Figure 13. Pleiotropic effects of broxbam. According to the present study, broxbam exerted anti-angiogenic functions, inhibited HDAC activity, disrupted cytoskeletal dynamics and induced apoptosis. HDAC, histone deacetylase.

which mimicked the effects of HDAC6 inhibition exerted by broxbam, led to a significant downregulation of proliferation markers Ki67 and E2F3. α -Tubulin is another non-histone substrate that can be deacetylated by HDAC6 (54,56,66). HDAC6-dependent deacetylation of tubulin has been reported to result in potent effects on cytoskeletal dynamics and cell migration (54,66,67). HDAC6 has also been previously associated with the function of microtubule dynamics and regulation of microtubule-dependent cell migration (54). In the present study, broxbam-treated liver cancer cells displayed profound alterations in their cytoskeleton components F-actin and microtubules. After microtubules become disrupted, f-actin stress fibres and focal adhesions are formed in response (68,69). The cytoskeletal effects of broxbam exceeded those mediated by vorinostat, which corresponded with the weaker inhibitory effects of vorinostat on HDAC6 activity.

Broxbam was also found to exert antiangiogenic effects *in vivo*, as shown by the suppression of SIV growth in the zebrafish embryos. This effect was visible already at nM concentrations, resembling the antiproliferative IC_{50} values of broxbam in liver cancer cells. Notably, the antiangiogenic effects of broxbam were not accompanied by signs of cardiotoxicity or impairments in the development of zebrafish embryos, which are known to be highly sensitive to toxic stress (70). The antiangiogenic effects of broxbam were likely to be due to a combination of mechanisms, with contributions from both pharmacophores contained within the structure of this chimeric compound. In this respect, HDACis are known to inhibit VEGF-induced angiogenesis *in vitro* as well as *in vivo* (71), such that CA-4-driven anti-angiogenesis has also been linked to the inhibition of VEGF (72). However, tumour vasculature disrupting agents, especially those derived from

CA4, have been shown to confer a high toxicity risk (59). Therefore, although broxbam contains a CA4-derived pharmacophore, it did not mediate toxic effects. This suggests that the effects of this novel chimeric compound may instead arise from its inhibitory effects on HDACs. The present study revealed that HDAC6-specific knockdown resulted in the downregulation of E2F3 expression in Huh7 cells. E2F3 is regarded to be a key factor for endothelial cell proliferation and angiogenesis (73). Therefore, it is conceivable that the pronounced HDAC6 inhibition of broxbam substantially contributed to its antiangiogenic effects due to the suppression of endothelial E2F3 expression. Further study is warranted to verify this hypothesis. The effects of broxbam on liver cancer cells revealed in the present study are summarized in Fig. 13.

Currently available treatment options for advanced and inoperable liver cancer are restricted to multi-kinase inhibitors, such as sorafenib or regorafenib (74). Although the therapeutic concentration of sorafenib is $\sim 8 \mu\text{M}$ (75), lower concentrations of broxbam was able to induce pronounced antitumor effects in the *in vivo* experiments with liver cancer xenografts on the CAM of fertilised chicken eggs. In addition to the therapeutic effects mediated by this low dosage of broxbam, which probably does not induce pronounced side effects, it also exhibited pronounced antineoplastic effects. This renders broxbam to be the experimental compound for alternative approaches for clinical liver cancer treatment.

The combination of HDACis and sorafenib has previously been demonstrated to exert enhanced anticancer activity and may therefore be an advantageous approach compared with sorafenib monotherapy (51,76,77). Freese *et al* previously reported that HDACi sensitised HCC cells to sorafenib treatment (78), which may be due to the overexpression of HDACs

in HCCs. In a recent review, Garmpis *et al* (51) highlighted the potential suitability of HDACis as anticancer agents and their application in combinatorial therapies for the enhanced treatment of HCC. Although the preclinical data of HDACi-based combination therapies are promising, these authors also reported results from a critical phase I clinical trial in which sorafenib was tested in combination with vorinostat in patients with liver cancer. Although some patients showed good tolerability and stable disease, this treatment also led to adverse toxicities in the majority of patients, which necessitated dose modifications and prevented progression towards phase 2 clinical trial (79). In the present study, results from the preclinical *in vitro* and *in vivo* studies suggest the suitability and tolerability of this chimeric hydroxamate-trimethoxystilbene conjugate for liver cancer treatment. The fact that signs of toxicity were observed in neither zebrafish embryos nor in the CAM, couple with the findings that the chicken embryos developed and survived, suggest that broxbam may exert fewer toxic effects compared with other HDACis, including vorinostat. Future studies involving the effects of combination therapies with broxbam and sorafenib should clarify this important issue. In addition, to address the suitability of broxbam for personalised therapeutic approaches, investigation of patient-derived primary liver cancer cells should be executed.

To conclude, the present study evaluated the recently-introduced chimeric inhibitor broxbam (20) for its potential anticancer activity in liver cancer cells and the underlying molecular mechanism. Additionally, its possible antitumoral and antiangiogenic effects were examined in *in vivo* settings by performing in chick embryo and zebrafish experiments. On the basis of the presented data, broxbam is implicated to be a promising chimeric HDACi that should be evaluated further as a potential compound for liver cancer treatment, either as a monotherapy or in combination with other clinically-relevant HCC therapeutics, such as sorafenib.

Acknowledgements

Not applicable.

Funding

The present study was funded by the Else Kröner-Fresenius-Stiftung Grant No. 2016 A47 (to AD).

Availability of data and materials

The datasets used and/or analysed during the current study are available from the corresponding author on reasonable request.

Authors' contributions

SIB: Investigation, zebrafish angiogenesis assay and data analysis. AD: Investigation, crystal violet assay, real-time inhibition of cell proliferation, lactate dehydrogenase (LDH) cytotoxicity assay, western blotting, reverse transcription-quantitative PCR (RT-qPCR), apoptosis detection, HDAC activity assay, immunofluorescence assay and scratch wound healing assay. GTA: Investigation, small-interfering (si)RNA assay, western blotting and RT-qPCR. MF: Western blotting

and RT-qPCR. AK: Investigation, crystal violet staining and LDH-Assay. LK: Investigation, crystal violet staining and LDH-Assay. BB: Conceptualisation, proof reading, validation. RS: Conceptualisation, validation and language proof reading. BN: Conceptualisation and CAM Assay. MH: Conceptualisation and validation and proof reading. All authors have read and agreed to the published version of the manuscript. SIB, BN, MF and AK confirm the authenticity of all the raw data.

Ethics approval and consent to participate

Not applicable.

Patient consent for publication

Not applicable.

Competing interests

The authors declare that they have no competing interests.

References

1. Siegel RL, Miller KD, Fuchs HE and Jemal A: Cancer statistics, 2021. *CA Cancer J Clin* 71: 7-33, 2021.
2. Mosconi S, Beretta GD, Labianca R, Zampino MG, Gatta G and Heinemann V: Cholangiocarcinoma. *Crit Rev Oncol Hematol* 69: 259-270, 2009.
3. Bray F, Ferlay J, Soerjomataram I, Siegel RL, Torre LA and Jemal A: Global cancer statistics 2018: GLOBOCAN estimates of incidence and mortality worldwide for 36 cancers in 185 countries. *CA Cancer J Clin* 68: 394-424, 2018.
4. Vogel A, Cervantes A, Chau I, Daniele B, Llovet JM, Meyer T, Nault JC, Neumann U, Rieke J, Sangro B, *et al*: Hepatocellular carcinoma: ESMO clinical practice guidelines for diagnosis, treatment and follow-up. *Ann Oncol* 29 (Suppl 4): iv238-iv255, 2018.
5. Lim H, Ramjessingh R, Liu D, Tam VC, Knox JJ, Card PB and Meyers BM: Optimizing survival and the changing landscape of targeted therapy for intermediate and advanced hepatocellular carcinoma: A systematic review. *J Natl Cancer Inst* 113: 123-136, 2021.
6. Li Y, Gao ZH and Qu XJ: The adverse effects of sorafenib in patients with advanced cancers. *Basic Clin Pharmacol Toxicol* 116: 216-221, 2015.
7. Tang W, Chen Z, Zhang W, Cheng Y, Zhang B, Wu F, Wang Q, Wang S, Rong D, Reiter FP, *et al*: The mechanisms of sorafenib resistance in hepatocellular carcinoma: Theoretical basis and therapeutic aspects. *Sig Transduct Target Ther* 5: 87, 2020.
8. Doherty B, Nambudiri VE and Palmer WC: Update on the diagnosis and treatment of cholangiocarcinoma. *Curr Gastroenterol Rep* 19: 2, 2017.
9. Morise Z, Sugioka A, Tokoro T, Tanahashi Y, Okabe Y, Kagawa T and Takeura C: Surgery and chemotherapy for intrahepatic cholangiocarcinoma. *World J Hepatol* 2: 58-64, 2010.
10. Goehringer N, Biersack B, Peng Y, Schobert R, Herling M, Ma A, Nitzsche B and Höpfner M: Anticancer activity and mechanisms of action of new chimeric EGFR/HDAC-inhibitors. *Int J Mol Sci* 22: 8432, 2021.
11. Biersack B, Polat S and Höpfner M: Anticancer properties of chimeric HDAC and kinase inhibitors. *Semin Cancer Biol*: Nov 12, 2020 (Epub ahead of print).
12. Park SY and Kim JS: A short guide to histone deacetylases including recent progress on class II enzymes. *Exp Mol Med* 52: 204-212, 2020.
13. Kaletsch A, Pinkerneil M, Hoffmann MJ, Jaguva Vasudevan AA, Wang C, Hansen FK, Wiek C, Hanenberg H, Gertzen C, Gohlke H, *et al*: Effects of novel HDAC inhibitors on urothelial carcinoma cells. *Clin Epigenetics* 10: 100, 2018.
14. Gong D, Zeng Z, Yi F and Wu J: Inhibition of histone deacetylase 11 promotes human liver cancer cell apoptosis. *Am J Transl Res* 11: 983-990, 2019.

15. Steinemann G, Dittmer A, Kuzyniak W, Hoffmann B, Schrader M, Schobert R, Biersack B, Nitzsche B and Höpfner M: Animacroxam, a novel dual-mode compound targeting histone deacetylases and cytoskeletal integrity of testicular germ cell cancer cells. *Mol Cancer Ther* 16: 2364-2374, 2017.
16. Manal M, Chandrasekar MJN, Gomathi Priya J and Nanjan MJ: Inhibitors of histone deacetylase as antitumor agents: A critical review. *Bioorg Chem* 67: 18-42, 2016.
17. Juan LJ, Shia WJ, Chen MH, Yang WM, Seto E, Lin YS and Wu CW: Histone deacetylases specifically down-regulate p53-dependent gene activation. *J Biol Chem* 275: 20436-20443, 2000.
18. Mann BS, Johnson JR, Cohen MH, Justice R and Pazdur R: FDA approval summary: Vorinostat for treatment of advanced primary cutaneous T-cell lymphoma. *Oncologist* 12: 1247-1252, 2007.
19. Streubel G, Schrepfer S, Kallus H, Parnitzke U, Wulff T, Herrmann F, Borgmann M and Hamm S: Histone deacetylase inhibitor resminostat in combination with sorafenib counteracts platelet-mediated pro-tumoral effects in hepatocellular carcinoma. *Sci Rep* 11: 9587, 2021.
20. Schmitt F, Gosch LC, Dittmer A, Rothemund M, Mueller T, Schobert R, Biersack B, Volkamer A and Höpfner M: Oxazole-bridged combretastatin A-4 derivatives with tethered hydroxamic acids: Structure-activity relations of new inhibitors of HDAC and/or tubulin function. *Int J Mol Sci* 20: 383, 2019.
21. Méndez-Callejas GM, Leone S, Tanzarella C and Antoccia A: Combretastatin A-4 induces p53 mitochondrial-relocalisation independent-apoptosis in non-small lung cancer cells. *Cell Biol Int* 38: 296-308, 2014.
22. Kim JH, Yoon EK, Chung HJ, Park SY, Hong KM, Lee CH, Lee YS, Choi K, Yang Y, Kim K and Kim IH: p53 acetylation enhances Taxol-induced apoptosis in human cancer cells. *Apoptosis* 18: 110-120, 2013.
23. Tron GC, Pirali T, Sorba G, Pagliai F, Busacca S and Genazzani AA: Medicinal chemistry of combretastatin A4: present and future directions. *J Med Chem* 49: 3033-3044, 2006.
24. Hesham HM, Lasheen DS and Abouzid KAM: Chimeric HDAC inhibitors: Comprehensive review on the HDAC-based strategies developed to combat cancer. *Med Res Rev* 38: 2058-2109, 2018.
25. Griggs J, Metcalfe JC and Hesketh R: Targeting tumour vasculature: The development of combretastatin A4. *Lancet Oncol* 2: 82-87, 2001.
26. Gaspari R, Prota AE, Bargsten K, Cavalli A and Steinmetz MO: Structural basis of cis- and trans-combretastatin binding to tubulin. *Chem* 2: 102-113, 2017.
27. Schaller E, Ma A, Gosch LC, Klefenz A, Schaller D, Goehringer N, Kaps L, Schuppan D, Volkamer A, Schobert R, *et al*: New 3-Aryl-2-(2-thienyl)acrylonitriles with high activity against hepatoma cells. *Int J Mol Sci* 22: 2243, 2021.
28. Nwosu ZC, Battello N, Rothley M, Piorońska W, Sitek B, Ebert MP, Hofmann U, Sleeman J, Wölfl S, Meyer C, *et al*: Liver cancer cell lines distinctly mimic the metabolic gene expression pattern of the corresponding human tumours. *J Exp Clin Cancer Res* 37: 211, 2018.
29. Kasai F, Hirayama N, Ozawa M, Satoh M and Kohara A: HuH-7 reference genome profile: Complex karyotype composed of massive loss of heterozygosity. *Hum Cell* 31: 261-267, 2018.
30. Nakabayashi H, Taketa K, Miyano K, Yamane T and Sato J: Growth of human hepatoma cells lines with differentiated functions in chemically defined medium. *Cancer Res* 42: 3858-3863, 1982.
31. Monteil M, Migianu-Griffoni E, Sainte-Catherine O, Di Benedetto M and Lecouvey M: Bisphosphonate prodrugs: Synthesis and biological evaluation in HuH7 hepatocarcinoma cells. *Eur J Med Chem* 77: 56-64, 2014.
32. Xu L, Hausmann M, Dietmaier W, Kellermeier S, Pesch T, Stieber-Gunckel M, Lippert E, Klebl F and Rogler G: Expression of growth factor receptors and targeting of EGFR in cholangiocarcinoma cell lines. *BMC Cancer* 10: 302, 2010.
33. Jo JR, An S, Ghosh S, Nedumaran B and Kim YD: Growth hormone promotes hepatic gluconeogenesis by enhancing BTG2-YY1 signaling pathway. *Sci Rep* 11: 18999, 2021.
34. Kuete V, Sandjo LP, Ouete JLN, Fouotsa H, Wiench B and Efferth T: Cytotoxicity and modes of action of three naturally occurring xanthenes (8-hydroxycudraxanthone G, morusinigin I and cudraxanthone I) against sensitive and multidrug-resistant cancer cell lines. *Phytomedicine* 21: 315-322, 2014.
35. Gillies RJ, Didier N and Denton M: Determination of cell number in monolayer cultures. *Anal Biochem* 159: 109-113, 1986.
36. Korzeniewski C and Callewaert DM: An enzyme-release assay for natural cytotoxicity. *J Immunol Methods* 64: 313-320, 1983.
37. Nitzsche B, Gloesenkamp C, Schrader M, Ocker M, Preissner R, Lein M, Zakrzewicz A, Hoffmann B and Höpfner M: Novel compounds with antiangiogenic and antiproliferative potency for growth control of testicular germ cell tumours. *Br J Cancer* 103: 18-28, 2010.
38. Sivandzade F, Bhalerao A and Cucullo L: Analysis of the mitochondrial membrane potential using the cationic JC-1 dye as a sensitive fluorescent probe. *Bio Protoc* 9: e3128, 2019.
39. Livak KJ and Schmittgen TD: Analysis of relative gene expression data using real-time quantitative PCR and the 2(-Delta Delta C(T)) method. *Methods* 25: 402-408, 2001.
40. Bobadilla AV, Arévalo J, Sarró E, Byrne HM, Maini PK, Carraro T, Balocco S, Meseguer A and Alarcón T: In vitro cell migration quantification method for scratch assays. *J R Soc Interface* 16: 20180709, 2019.
41. Almeida VM, Bezerra MA Jr, Nascimento JC and Amorim LMF: Anticancer drug screening: Standardization of in vitro wound healing assay. *J Bras Patol Med Lab* 55: 606-619, 2019.
42. Serbedzija GN, Flynn E and Willett CE: Zebrafish angiogenesis: A new model for drug screening. *Angiogenesis* 3: 353-359, 1999.
43. Warburg O: On the origin of cancer cells. *Science* 123: 309-314, 1956.
44. Thorens B: GLUT2, glucose sensing and glucose homeostasis. *Diabetologia* 58: 221-232, 2015.
45. Kaufmann SH and Earnshaw WC: Induction of apoptosis by cancer chemotherapy. *Exp Cell Res* 256: 42-49, 2000.
46. Reers M, Smiley ST, Mottola-Hartshorn C, Chen A, Lin M and Chen LB: Mitochondrial membrane potential monitored by JC-1 dye. *Methods Enzymol* 260: 406-417, 1995.
47. Kim R, Emi M and Tanabe K: Role of mitochondria as the gardens of cell death. *Cancer Chemother Pharmacol* 57: 545-553, 2006.
48. Fridman JS and Lowe SW: Control of apoptosis by p53. *Oncogene* 22: 9030-9040, 2003.
49. Kim R, Tanabe K, Uchida Y, Emi M, Inoue H and Toge T: Current status of the molecular mechanisms of anticancer drug-induced apoptosis. The contribution of molecular-level analysis to cancer chemotherapy. *Cancer Chemother Pharmacol* 50: 343-352, 2002.
50. Giaginis C, Damaskos C, Koutsounas I, Zizi-Serbetzoglou A, Tsoukalas N, Patsouris E, Kouraklis G and Theocharis S: Histone deacetylase (HDAC)-1, -2, -4 and -6 expression in human pancreatic adenocarcinoma: Associations with clinicopathological parameters, tumor proliferative capacity and patients' survival. *BMC Gastroenterol* 15: 148, 2015.
51. Garmpis N, Damaskos C, Garmpi A, Georgakopoulou VE, Sarantis P, Antoniou EA, Karamouzis MV, Nonni A, Schizas D, Diamantis E, *et al*: Histone deacetylase inhibitors in the treatment of hepatocellular carcinoma: Current evidence and future opportunities. *J Pers Med* 11: 223, 2021.
52. Scholzen T and Gerdes J: The Ki-67 protein: From the known and the unknown. *J Cell Physiol* 182: 311-322, 2000.
53. Kim HR, Rahman FU, Kim KS, Kim EK, Cho SM, Lee K, Moon OS, Seo YW, Yoon WK, Won YS, *et al*: Critical roles of E2F3 in growth and musculo-skeletal phenotype in mice. *Int J Med Sci* 16: 1557-1563, 2019.
54. Hubbert C, Guardiola A, Shao R, Kawaguchi Y, Ito A, Nixon A, Yoshida M, Wang XF and Yao TP: HDAC6 is a microtubule-associated deacetylase. *Nature* 417: 455-458, 2002.
55. Garcin C and Straube A: Microtubules in cell migration. *Essays Biochem* 63: 509-520, 2019.
56. Schaks M, Giannone G and Rottner K: Actin dynamics in cell migration. *Essays Biochem* 63: 483-495, 2019.
57. Norouzzadeh M, Kalikias Y, Mohammadpour Z, Sharifi L and Mahmoudi M: Determining population doubling time and the appropriate number of HepG2 cells for culturing in 6-well plate. *IJBAR* 10: 299-303, 2016.
58. Deng B, Luo Q, Halim A, Liu Q, Zhang B and Song G: The antiangiogenesis role of histone deacetylase inhibitors: Their potential application to tumor therapy and tissue repair. *DNA Cell Biol* 39: 167-176, 2020.
59. Tomaszewska B, Muzolf M, Grabysa R and Bodnar L: Cardiotoxicity of antiangiogenic drugs: Causes and mechanisms. *OncoReview* 11: 12-18, 2021.
60. Oda K, Arakawa H, Tanaka T, Matsuda K, Tanikawa C, Mori T, Nishimori H, Tamai K, Tokino T, Nakamura Y and Taya Y: p53AIP1, a potential mediator of p53-dependent apoptosis, and its regulation by Ser-46-phosphorylated p53. *Cell* 102: 849-862, 2000.

61. Matsuda K, Yoshida K, Taya Y, Nakamura K, Nakamura Y and Arakawa H: p53/AIP1 regulates the mitochondrial apoptotic pathway. *Cancer Res* 62: 2883-2889, 2002.
62. Porter AG and Jänicke RU: Emerging roles of caspase-3 in apoptosis. *Cell Death Differ* 6: 99-104, 1999.
63. Lee YR and Park SY: P53 expression in hepatocellular carcinoma: Influence on the radiotherapeutic response of the hepatocellular carcinoma. *Clin Mol Hepatol* 21: 230-231, 2015.
64. Li T, Zhang C, Hassan S, Liu X, Song F, Chen K, Zhang W and Yang J: Histone deacetylase 6 in cancer. *J Hematol Oncol* 11: 111, 2018.
65. Aldana-Masangkay GI and Sakamoto KM: The role of HDAC6 in cancer. *J Biomed Biotechnol* 2011: 875824, 2011.
66. Gao Y, Hubbert CC, Lu J, Lee YS, Lee JY and Yao TP: Histone deacetylase 6 regulates growth factor-induced actin remodeling and endocytosis. *Mol Cell Biol* 27: 8637-8647, 2007.
67. Tran AD-A, Marmo TP, Salam AA, Che S, Finkelstein E, Kabarriti R, Xenias HS, Mazitschek R, Hubbert C, Kawaguchi Y, *et al*: HDAC6 deacetylation of tubulin modulates dynamics of cellular adhesions. *J Cell Sci* 120: 1469-1479, 2007.
68. Enomoto T: Microtubule disruption induces the formation of actin stress fibers and focal adhesions in cultured cells: Possible involvement of the rho signal cascade. *Cell Struct Funct* 21: 317-326, 1996.
69. Liu BP, Chrzanowska-Wodnicka M and Burridge K: Microtubule depolymerization induces stress fibers, focal adhesions, and DNA synthesis via the GTP-binding protein Rho. *Cell Adhes Commun* 5: 249-255, 1998.
70. Zhang C, Willett C and Fremgen T: Zebrafish: An animal model for toxicological studies. *Curr Protoc Toxicol* 17: 1.7.1-1.7, 2003.
71. Deroanne CF, Bonjean K, Servotte S, Devy L, Colige A, Clausse N, Blacher S, Verdin E, Foidart JM, Nusgens BV and Castronovo V: Histone deacetylases inhibitors as anti-angiogenic agents altering vascular endothelial growth factor signaling. *Oncogene* 21: 427-436, 2002.
72. Su M, Huang J, Liu S, Xiao Y, Qin X, Liu J, Pi C, Luo T, Li J, Chen X and Luo Z: The anti-angiogenic effect and novel mechanisms of action of Combretastatin A-4. *Sci Rep* 6: 28139, 2016.
73. Zhou J, Cheng M, Wu M, Boriboun C, Jujo K, Xu S, Zhao TC, Tang YL, Kishore R and Qin G: Contrasting roles of E2F2 and E2F3 in endothelial cell growth and ischemic angiogenesis. *J Mol Cell Cardiol* 60: 68-71, 2013.
74. Heo YA and Syed YY: Regorafenib: A review in hepatocellular carcinoma. *Drugs* 78: 951-958, 2018.
75. Labeur TA, Hofsink Q, Takkenberg RB, van Delden OM, Mathôt RAA, Schinner R, Malfertheiner P, Amthauer H, Schütte K, Basu B, *et al*: The value of sorafenib trough levels in patients with advanced hepatocellular carcinoma-a substudy of the SORAMIC trial. *Acta Oncol* 59: 1028-1035, 2020.
76. Yuan H, Li AJ, Ma SL, Cui LJ, Wu B, Yin L and Wu MC: Inhibition of autophagy significantly enhances combination therapy with sorafenib and HDAC inhibitors for human hepatoma cells. *World J Gastroenterol* 20: 4953-4962, 2014.
77. Bitzer M, Horgner M, Giannini EG, Ganten TM, Wörns MA, Siveke JT, Dollinger MM, Gerken G, Scheulen ME, Wege H, *et al*: Resminostat plus sorafenib as second-line therapy of advanced hepatocellular carcinoma-The SHELTER study. *J Hepatol* 65: 280-288, 2016.
78. Freese K, Seitz T, Dietrich P, Lee SML, Thasler WE, Bosserhoff A and Hellerbrand C: Histone deacetylase expressions in hepatocellular carcinoma and functional effects of histone deacetylase inhibitors on liver cancer cells in vitro. *Cancers (Basel)* 11: 1587, 2019.
79. Gordon SW, McGuire WP III, Shafer DA, Sterling RK, Lee HM, Matherly SC, Roberts JD, Bose P, Tombes MB, Shrader EE, *et al*: Phase I study of sorafenib and vorinostat in advanced hepatocellular carcinoma. *Am J Clin Oncol* 42: 649-654, 2019.



This work is licensed under a Creative Commons Attribution-NonCommercial-NoDerivatives 4.0 International (CC BY-NC-ND 4.0) License.